INVESTIGATION OF STRUCTURAL AND ELECTROCHEMICAL PROPERTIES OF BIOMASS BASED ACTIVATED CARBON MATERIALS FOR ENERGY STORAGE APPLICATIONS

A THESIS SUBMITTED TO

THE GRADUATE SCHOOL OF NATURAL AND APPLIED SCIENCES
OF
MIDDLE EAST TECHNICAL UNIVERSITY

BY

KADİR ÖZGÜN KÖSE

IN PARTIAL FULFILLMENT OF THE REQUIREMENTS
FOR
THE DEGREE OF MASTER OF SCIENCE
IN
METALLURGICAL AND MATERIALS ENGINEERING

SEPTEMBER 2017

Approval of the thesis:

INVESTIGATION OF STRUCTURAL AND ELECTROCHEMICAL PROPERTIES OF BIOMASS BASED ACTIVATED CARBON MATERIALS FOR ENERGY STORAGE APPLICATIONS

submitted by **KADİR ÖZGÜN KÖSE** in partial fulfillment of the requirements for the degree of **Master of Science in Metallurgical and Materials Engineering Department, Middle East Technical University** by,

Prof. Dr. Gülbin Dural Ünver _____
Dean, Graduate School of **Natural and Applied Science**

Prof. Dr. C. Hakan Gür _____
Head of Department, **Metallurgical and Materials Engineering**

Prof. Dr. Kadri Aydınol _____
Supervisor, **Metallurgical and Materials Eng. Dept., METU**

Examining Committee Members:

Prof. Dr. İshak Karakaya _____
Metallurgical and Materials Engineering Dept., METU

Prof. Dr. Kadri Aydınol _____
Metallurgical and Materials Engineering Dept., METU

Prof. Dr. Zafer Evis _____
Engineering Sciences Dept., METU

Assoc. Prof. Dr. Emrah Ünalan _____
Metallurgical and Materials Engineering Dept., METU

Assist. Prof. Dr. Emre Taşcı _____
Physics Engineering Dept., Hacettepe University

Date: 05.09.2017

I hereby declare that all information in this document has been obtained and presented in accordance with academic rules and ethical conduct. I also declare that, as required by these rules and conduct, I have fully cited and referenced all material and results that are not original to this work.

Name, Last name: Kadir Özgün, Köse

Signature :

ABSTRACT

INVESTIGATION OF STRUCTURAL AND ELECTROCHEMICAL PROPERTIES OF BIOMASS BASED ACTIVATED CARBON MATERIALS FOR ENERGY STORAGE APPLICATIONS

KÖSE, Kadir Özgün

M. Sc., Department of Metallurgical and Materials Engineering

Supervisor: Prof. Dr. M. Kadri Aydınol

September 2017, 86 pages

Finding new energy sources and efficient ways for energy storage is one of the primary goals in both scientific and industrial research. To achieve this purpose, studies are concentrated on optimizing the characteristics of energy storage devices such as batteries, fuel cells and supercapacitors. Activated carbon (AC), beside its versatile application areas including wastewater and gas treatment, is used as electrodes in electrical double layer capacitors and as cathode in metal air batteries due to its high conductivity and high specific surface area (up to 3000 m^2/g). In this thesis, AC is derived from biomass like pine cone, and its structural and electrochemical properties were characterized as an electrode material in supercapacitors.

The porosity and conductivity of AC have a great influence on the electrochemical properties when used in EDLC applications; therefore, the production conditions of AC were arranged accordingly. As a result, surface area range of 1300 to 2700 m^2/g was achieved. Furthermore, it is seen that electrical conductivity of AC is dependent on activation temperature with a 5 orders of magnitude greater value for high

temperature treated ones. This dependence is linked to surface functional groups and structural order of the AC's and they are characterized by FTIR and Raman spectroscopies. After the production and characterization of AC's with various properties, they were used in the EDLC fabrication with two binders and two electrolytes. The effect of binders and electrolytes were investigated in EDLC performance; PSBR100 binder is found to be suitable for high power applications, whereas LA 132 binder is appropriate for high energy devices. The performance of TEA BF_4 salt in acetonitrile was superior to TBA PF_6 in acetonitrile. As a result, maximum power density of 72 kW/kg and energy density of 28 Wh/kg were achieved in EDLC's fabricated.

Keywords: Activated carbon, EDLC, organic electrolyte, chemical activation.

ÖZ

ENERJİ DEPOLAMA UYGULAMALARI İÇİN BİYOKÜTLE ESASLI AKTİF KARBON MALZEMELERİNİN YAPISAL VE ELEKTROKİMYASAL ÖZELLİKLERİNİN İNCELENMESİ

KÖSE, Kadir Özgün

Yüksek Lisans, Metalurji ve Malzeme Mühendisliği Bölümü

Tez Yöneticisi: Prof. Dr. M. Kadri Aydınol

Eylül 2017, 86 sayfa

Yeni enerji kaynakları ve enerji depolama için etkili yöntemler bulmak bilimsel ve sanayiye yönelik araştırmaların temel amaçlarından biridir.Bu amaca ulaşmak için, çalışmalar, bataryalar, yakıt hücreleri ve süperkapasitörlerin özelliklerini optimize etmeye odaklanmıştır. Aktif Karbon (AC), atık su ve gaz arıtma gibi çeşitli uygulama alanlarının yanında, yüksek iletkenlik ve spesifik yüzey alanından dolayı (3000 m^2/g a kadar), elektriksel çift tabaka kapasitörlerin elektrotları ve metal hava bataryalarının katodu olarak kullanılır. Bu çalışmanın amacı fıstık çamı kozalağı gibi biyokütlelerden aktif karbonu elde etmek ve elektrot olarak kullanılacak bu malzemenin yapısal ve elektrokimyasal özelliklerini belirlemektir.

Aktif karbonlar EDLC uygulamalarında kullanıldıklarında gözenek durumu ve elektriksel iletkenliğin elektrokimyasal davranışa büyük etkisi vardır; bu sebeple aktif karbon üretim süreci buna göre ayarlanmıştır. Sonuç olarak, 1300-2700 m^2/g aralığında yüzey alanı elde edilmiştir. Buna ek olarak, aktivasyon sıcaklığının elektriksel iletkenliğe, yüksek sıcaklığa maruz kalanların 10 000 kat fazla olacak kadar etkisi olduğu gözlenmiştir. Bu bağlılık yüzey fonksiyonel grupları ve yapısal

düzenle ilişkilendirilmiş ve FTIR ve Raman spektroskopileriyle karakterize edilmiştir. Çeşitli özelliklerdeki aktif karbonlar üretildikten sonra, bunlar iki bağlayıcı ve iki elektrolitle birlikte EDLC yapımında kullanılmıştır. Bağlayıcı ve elektrolitin EDLC performansına etkisi ayrıca irdelenmiş ve PSBR 100 bağlayıcının yüksek güç uygulamaları için uygun olduğu, LA 132 bağlayıcının ise enerji yoğunluğunu artırmak için kullanılabileceği sonucuna varılmıştır. Bunun yanında, asetonitril içinde TEA BF_4 tuzunun EDLC performansının asetonitril içinde TBA PF_6 tuzundan iyi olduğu gözlenmiştir. Sonuç olarak, üretilen EDLC'lerde 72 kW/kg maximum güç yoğunluğu ve 28 Wh/kg enerji yoğunluğu elde edlimiştir.

Anahtar Kelimeler: Aktif karbon, EDLC, organik elektrolit, kimyasal aktivasyon.

To my family

ACKNOWLEDGEMENTS

Firstly, I want to start with appreciation to my first advisor Prof. Dr. Şakir BOR. His life style and understanding of science deeply influenced me and decisions about my academic career. I want to honor his memory and thank him for all impressions of him in my life.

I also want to thank Prof. Dr. Kadri AYDINOL, for all contributions to my knowledge about in this study. His guidance inspired me to work harder and solve the problems.

I appreciate my lab group, Ayşegül AFAL GENİŞ, Berke PİŞKİN, Burcu ARSLAN, Burcu MİSER, Vahit KURT, Emre YILMAZ and Cansu SAVAŞ, who always helped me in laboratory, as well as in my personal life with their friendship.

I want to thank to my parents Ahmet and Zarife KÖSE, who always supported my decisions and worked for my well-being in all their lives.

Lastly, I want to thank to Merve BESCİ, whose endless love kept me strong facing with all my problems.

TABLE OF CONTENTS

LIST OF TABLES

TABLES

LIST OF FIGURES

FIGURES

CHAPTER 1

INTRODUCTION

The demand for designing new electrochemical energy storage systems or optimizing the existing ones is increasing due to the necessity of reducing fossil fuel consumption. Electrical double layer capacitor (EDLC) takes an important place among other energy storage devices considering its efficient energy storage mechanism and prolonged cycle life. It is characteristically a high power device, suffering from low energy density. The increasing use of EDLC mainly depends on enhancement of its energy density. Therefore, optimizing the properties of EDLC is of paramount importance for both scientific and technological research.

After the first utilization of electrostatic charge storage mechanism to construct an energy storage device (Leyden jars), capacitor technology has grown up with the application of electrostatic (dielectric) capacitors. The construction of dielectric capacitor includes two parallel metal plates and a dielectric material that does not allow electronic conduction. Later, electrolytic capacitors are invented and introduced into the market. They make use of two aluminum plates with Al_2O_3 layer on the surfaces of them and an electrolyte. Since charge storage is only at the oxide layer, which is much thinner compared to dielectric material in dielectric capacitors, capacitance is significantly enhanced. However, capacitance supplied by electrolytic capacitor is still not enough to meet energy requirements. Then, electrical double layer capacitors are developed, using the ion electroadsorption at electrode electrolyte interface; namely, the double layer. They store much more energy than the electrolytic capacitors; also their power is superior to batteries.

Application areas of EDLC's include power electronic devices, memory protection, hybrid cars and military applications (such as pulsed weapons and lasers) [1, 2]. They are generally regarded as complementary devices to batteries;

however, when the power of the device is particularly critical in an application, EDLC is generally chosen among other electrochemical energy storage devices [3].

Before going into details of conditions that determine EDLC performance, this chapter focuses on basics of capacitive energy storage and general properties of electrochemical capacitors.

1.1. Capacitive Energy Storage

A capacitor is a two-terminal electrical component used to store energy in an electric field. If a potential is applied across the conductors, an electric field develops in the dielectric. This causes charge separation, positive charge to collect on one plate and negative charge on the other plate. The insulating layer between a capacitor's plates is commonly called the dielectric. Due to this insulating layer, DC current cannot flow through the capacitor. As the name implies, the most important property of a capacitor is its capacitance. This gives the ability to store charge on the plates of a capacitor.

Capacitance is defined by stored charge per applied voltage. It has a unit of farad, which is equivalent to coulombs per volt. Capacitance is an intrinsic property of a capacitor, like resistance of a resistor, which means that it does not change with changing electrical parameters. It is related with its permittivity of dielectric, electrode area and distance between electrodes by:

$$\mathbf{C} = \boldsymbol{\varepsilon_r \varepsilon_0} \frac{\boldsymbol{A}}{\boldsymbol{l}} \quad \text{.....(1)}$$

,where C is capacitance, ε_r is relative permittivity of the dielectric, ε_0 is permittivity of perfect vacuum, A is electrode surface area, and l is distance between electrodes. Permittivity of perfect vacuum, ε_0, is 8.85 x 10^{-12} F/m, and permittivities of dielectrics are given relative to this value, ε_r, by dividing permittivity of the

dielectric to that of perfect vacuum. Therefore, product of these gives the permittivity of the medium used in the capacitor construction. As a consequence, this equation implies that in order to increase capacitance, increasing dielectric constant and surface area of electrodes and decreasing distance between electrodes are essential features.

1.2. Electrochemical Capacitors

After the first patent of Becker in 1957 [4] on EDLC's with two porous carbon electrodes, progress on the subject gives rise to confusion on the terminology. While some groups used "supercapacitor" to this growing research area, the others gave the name "ultracapacitor". Burke proposed "electrochemical capacitor" and it is generally accepted to define the name of electrochemical systems that utilize capacitive energy storage [5], including EDLC's, pseudo capacitors and hybrid capacitors.

EDLC is invented earliest and its charge storage mechanism is simpler than other electrochemical capacitors. Ion accumulation as a result of applied voltage is the capacitive charge storage mechanism. In pseudo capacitors, besides ion accumulation, reversible faradaic reactions take place at electrode surface, which brings about higher capacitance values than EDLC. Hybrid capacitor, on the other hand, utilizes both capacitive energy storage and battery type redox reactions. It has one battery type electrode (generally for Li^+ intercalation) and one capacitive electrode [6].

Figure 1 is generally called as "Ragone plot". It is a graph of specific power versus specific energy, reflecting the energy and power characteristics of an energy storage device. It is seen that power characteristics of a supercapacitor is superior to batteries; however, energy densities are low. The reason is charge storage mechanism: batteries use redox reactions for energy, having kinetic barriers such as diffusion of ions to electrode surface and electron transfer at the electrode. EDLC is based on accumulation of ions at the double layer, and corresponding

non-faradaic current. It is also seen that electrochemical capacitors have broad region on the diagram, this is because energy densities can be increased by introducing fast redox reactions, and it is the principle of pseudo-capacitors. Furthermore, energy density can be still increased using hybrid configurations. Using Li^+ intercalation anodes brings about nearly an energy density of a battery.

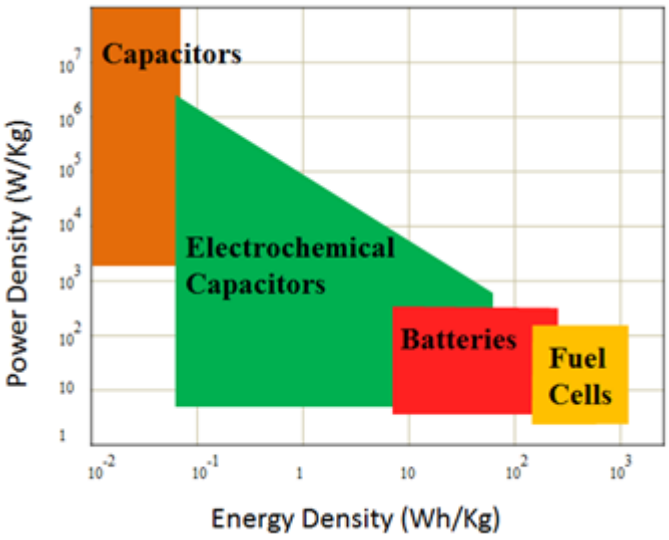

Figure 1. Ragone plot for different electrochemical systems.

1.2.1. Electrical Double Layer Capacitors (EDLC's)

EDLC's are based on charge separation on two polarizable electrodes with the formation of electrical double layer in the electrode-electrolyte interface. The working principle is similar to conventional dielectric capacitors; except the formation and utilization of the electrical double layer, see Figure 2. The dielectric material is replaced with an electrolyte (a salt dissolved in a solvent), which also prevents electronic conduction but permit ionic conduction.

Conventional capacitors make use of two metal plates and an insulating material between them. Charge separation upon applied voltage causes capacitive charge storage within the plates. As distance between the electrodes is determined by the

thickness of the insulating material, this distance cannot be as small as the distance between ions and electrode surface when the double layer is formed. Moreover, electrode materials used in electrochemical capacitors are porous; they have large surface area.

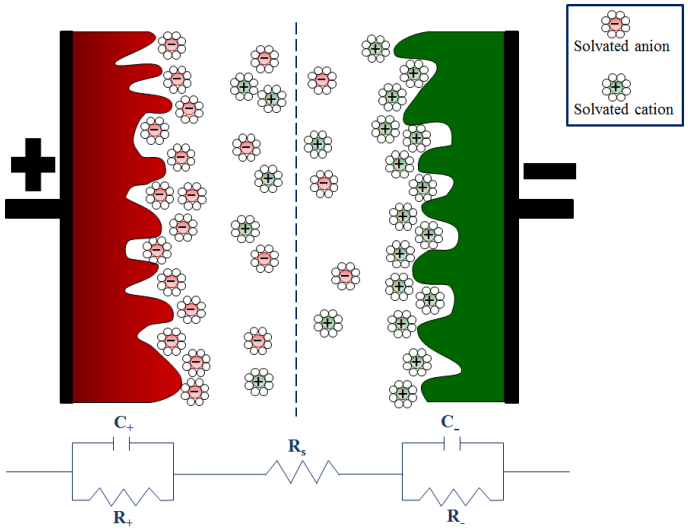

Figure 2. Schematic drawing of electrodes in capacitor and equivalent circuit model.

If this type of a configuration is connected to a power supply and a potential applied, electrical double layer is formed. As one can see from the Figure 2, charge separation occurs on the surface of the electrodes, so that we have 2 capacitors, having very small spacing, connected in series. Since the spacing of the charge separation is very small, in the order of nanometers, capacitance values are very high like 100 Farad per gram. It is microfarads in usual capacitors. Therefore, they are named as ultra or supercapacitors.

EDLC's have two porous polarizable electrodes. They rely on the principle of reversible electrostatic accumulation of ions on the surface of porous electrode. In charging, electrons move from positive to negative electrode, while in discharging, they move from negative to positive electrode. Considering size of the ions that

accumulates on the electrode surface, porous structure of the electrode must be tuned for matching ion size and effective ion electroadsorption. Due to very small spacing of the double layer, high specific capacitances (10 μF/cm^2) are achieved. Using porous materials (generally carbon) that have about 1000 m^2/g surface area, 100F/g gravimetric capacitance can be obtained. The stored energy of a capacitor is given by:

$$\boldsymbol{E = \frac{1}{2} C V^2} \quad \text{.....(2)}$$

, where *E* is energy supplied by an EDLC, *C* is capacitance, and *V* is potential region of electrochemical stability. Energy and capacitance is generally expressed in specific energy and capacitance units. To increase stored energy, capacitance and stability potential window must be increased. Stability potential window is determined by electrolyte, for example, it is 1.23 V for aqueous electrolytes (water decomposition).

The maximum power of a capacitor is given by:

$$\boldsymbol{P = \frac{V^2}{4\,ESR}} \quad \text{.....(3)}$$

, where *P* is maximum power of an EDLC, *ESR* is equivalent series resistance, sum of the ionic resistance of the electrolyte, the electronic resistance of electrodes, and interface resistances between electrodes and current collectors.

Based on the characteristics of the double layer briefly given above, deriving active material from biomass and construction of EDLC's with optimized power and energy density are the main purposes of this study. Surface area, pore size distribution and electrical conductivity are the key factors of the performance of active material in EDLC's; therefore, processing parameters for active material production from biomass are determined in order to manipulate these characteristics of active material. Furthermore, properties of the active material

must match characteristics of the ions in the electrolyte, so that different electrolytes are used in EDLC construction. Electrode preparation (especially binder) also plays an important role in the power and energy density of the EDLC's; hence, the effect of different binders in electrode preparation has been investigated.

CHAPTER 2

LITERATURE REVIEW

2.1. Double Layer Models

Theoretical models for electrically charged interfaces date back to 19th century. The term double layer is coined after the work of Helmholtz, who suggests there is excess or deficiency of charge on an electrode surface when the oppositely charged ions are electrosorbed, see Figure 3 (a). He realized when a voltage is applied to a conductor that is in contact with an electrolyte, the surface of the conductor is charged. The charge on the surface is balanced with counterions in the electrolyte. In this model, this charge separation at the electrode-solution interface was expressed in the same way as a parallel plate capacitor. Although Helmholtz model has historical importance, it is criticized for not representing the real picture accurately; capacitance seems to be independent of voltage and electrolyte concentration, which is in contradiction with both theoretical and experimental studies [7].

In a more refined model, Gouy and Chapman proposed that thermal processes are in competition with electrostatic forces in proximity of electrode-solution interface, resulting in the formation of "*diffuse layer"* of charge, as one can see in Figure 3 (b). The concentration of excess charge is getting higher near the electrode surface, as electrostatic forces dominate over thermal fluctuations. Furthermore, the thickness of the diffuse layer depends on electrolyte concentration and potential, increasing both of which gives rise to compaction of the diffuse layer. In this model, since ions are assumed as point charges and they get close to surface disregarding physical limitations, calculated capacitance values are found to be unrealistically high.

The size of the ions is taken into consideration in the model of Stern. He combined the two previous double layer models of Helmholtz, and Gouy and Chapman. In the model, a plane of adsorbed charges (Helmholtz model) and decreasing charge density with increasing distance from the interface (Gouy-Chapman model) are both postulated. Consequently, overall capacitance of an electrode is suggested to have contributions from both the Helmholtz plane of adsorbed charges and diffuse layer of Gouy-Chapman model. The smaller capacitance value dominates, because they are assumed to behave two capacitors connected in series:

$$\frac{1}{C} = \frac{1}{C_H} + \frac{1}{C_d} \quad \text{.....(4)}$$

, where C is capacitance, C_H is capacitance resulting from Helmholtz plane, and C_d is capacitance from diffuse layer.

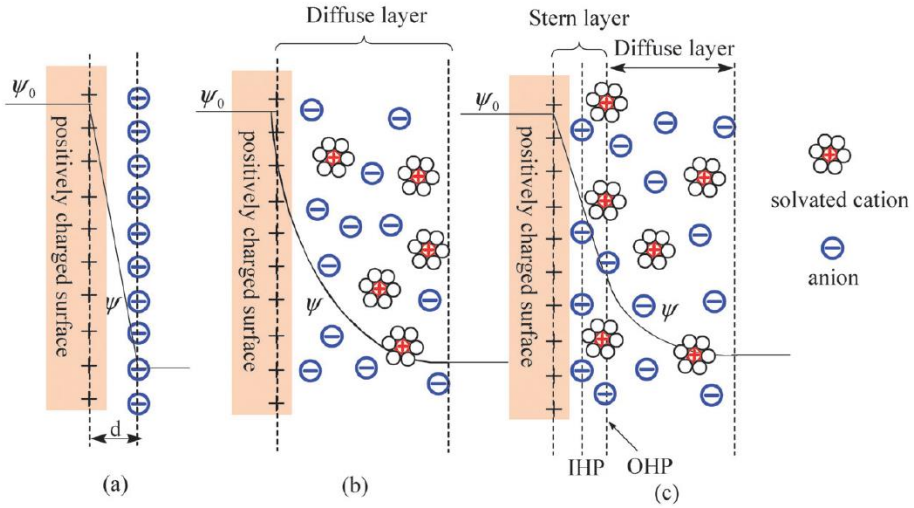

Figure 3. Schematic drawing of double layer models a) Helmholtz model, b) Gouy-Chapman model, c) Stern model [8].

2.2. Electrolytes for EDLC

There are three main types of electrolytes used in EDLC's: aqueous electrolytes, organic electrolytes and ionic liquids. The choice of electrolyte primarily depends on two criteria; electrochemical stability window and ionic conductivity. The other parameters include thermal stability, matching the properties of the materials used in construction of EDLC (active material, binder, current collector etc.), viscosity, toxicity and cost.

2.2.1. Aqueous Electrolytes

The most widely used aqueous electrolytes in EDLC applications are 1 M sulfuric acid (H_2SO_4) and 6 M potassium hydroxide (KOH) solutions. The conductivities of these electrolytes are 0.8 and 0.6 S/cm, respectively [9]. These values are an order of magnitude higher than that of organic electrolytes, giving rise to low ESR values. Furthermore, reported capacitance values are higher than those obtained with organic electrolytes. This is attributed to smaller ion sizes and higher dielectric constants of the aqueous electrolytes. However, aqueous electrolytes suffer from narrow electrochemical stability window; they are limited to 1.23 V, thermodynamic limit for water decomposition. Considering the effect of voltage on the energy and power density of an EDLC, this voltage limitation deteriorates the performance of aqueous electrolytes compared to the organic ones with stability windows up to 2.7-2.8 V.

2.2.2. Organic Electrolytes

Although scientific research mainly focused on EDLC's with aqueous electrolytes in recent years, commercial use of organic electrolytes are far more profound. The main advantage of using organic electrolytes in EDLC is its wide electrochemical stability window (2.7-2.8 V). Therefore, EDLC's with organic electrolytes

typically have high energy densities. They consist of an aprotic solvent like acetonitrile and propylene carbonate, and generally a quaternary ammonium salt dissolved in the solvent. The most widely used one is 1 M tetraethyl ammonium tetrafluoroborate (TEA BF_4, $(C_2H_5)_4BF_4$) in acetonitrile. The reason of choice depends on the solubility of the salt in the electrolyte and the ionic conductivity. However, even in the optimized conditions, the conductivity of 1 M ACN-TEA BF_4 solution is 0.06 S/cm, resulting in a higher ESR value than EDLC's with aqueous electrolytes [9].

2.2.3. Ionic Liquids

Ionic liquids are low temperature molten salts that give the opportunity to have a solvent free electrolyte, with only cations and anions without their solvation shells. The use of ionic liquids in electrochemical capacitors is relatively new, and implementations on this area is not mature enough so far. They have a very good thermal and electrochemical stability. They can reach operation temperature and voltage window of 300 °C and 6 V, respectively [10]. However, their ionic conductivities are typically very low, being the most important parameter that limits their use as electrochemical capacitor electrolytes [11]. Even one of the most conductive ionic liquid, $EMIMBF_4$ (1-Ethyl-3-Methylimidazolium tetrafluoroborate) has a conductivity of 0.0014 S/cm at 25 °C [9].

2.3. Binders for EDLC

Energy and power characteristics of EDLC's depend on several factors, such as porous structure and intrinsic conductivity of active material, electrolyte used, design of the cell, and electrode preparation. Utilization of appropriate binder and processing it effectively are the key factors to optimize the performance of EDLC's. Polymeric binders have a role to get a compact composite of active

material and conductive additive, which are in contact with current collector. Resistance due to this contact is one of the main contributions to ESR. Furthermore, blockage of porous structure with binder hinders the double layer formation and reduces capacitance [12]. Therefore, choice of binder is an important parameter in EDLC fabrication regarding both power and energy density.

The most widely used binders for EDLC applications are polyvinylidenedifluoride (PVDF), polytetrafluoroethylene (PTFE), sodium carboxymethyl cellulose (CMC), and styrene butadiene rubber (SBR). Besides, a polyacrylonitrile and styrene butadiene rubber based LA 135 binder is used in EDLC construction recently [13]. Among them, PVDF is widely used in both EDLC and Li ion battery applications. However, its solvent is N-methyl pyrrolidone (NMP), which is volatile and toxic and using it is not desirable. Besides, PTFE and PVDF binders are compared in a study based on EDLC applications [12], and PVDF is reported to block the porous structure more than PTFE. Still, electrode preparation with PTFE binder is troublesome, since it has an adhesion problem to current collector [14]. In the study of Sun *et. al.* [13], in which LA 135 is proposed as a novel binder for EDLC, effects of PTFE, CMC+SBR, LA 135 and PVDF binders on EDLC performance are compared. EDLC with LA 135 binder is reported to have the largest specific capacitance; however, its resistance is significantly larger than that with PTFE and CMC+SBR binders. EDLC with CMC+SBR binder has the lowest specific capacitance; but, its low resistance is suitable for high power applications. Furthermore, LA 132 binder (based on polyacrylonitrile like LA 135), is used for cathode of Li ion and Li-S batteries and displays promising properties [15, 16]. Yet, systematic investigation of its properties in EDLC applications is lacking in literature.

2.4. Electrode Materials for EDLC

Two main criteria must be met for a material in order to get sound results in EDLC applications that are high specific surface area and electronic conductivity [17]. With a tunable structure and chemistry, various forms of carbon satisfy these criteria. They have also good corrosion resistance, particularly important for improved cycle life of an EDLC. Their cost can be varied in a very broad scale, depending on the processing conditions and precursor materials. AC, the cheapest one, is by far the most widely used electrode material in EDLC applications. Besides, carbide derived carbons, templated carbons, carbon nanotubes, carbon onions, graphene and carbon aerogels have been utilized as electrode materials in EDLC applications [18].

2.5. Activated Carbon (AC)

AC is a disordered carbon form having very small (in the order of a few angstroms to several nanometers) pores. Such small pores result in a very large surface area, typically as high as 1500 m^2/g. The precursors for AC production include natural substances like pitch, coke, wood, coconut, sucrose, and synthetic materials such as polyvinyl chloride, polyacrylonitrile, polyaniline. These organic precursors are subjected to a treatment named as activation, in which they lose most of their H and O atoms, resulting in carbonaceous and also porous structure.

2.5.1. Activation Mechanisms

There are two activation processes used in AC production: physical (thermal) activation and chemical activation as given in Figure 4. In physical activation, precursor material is carbonized in an inert atmosphere first, and then activated using steam or carbon dioxide (CO_2). In chemical activation, precursor is

impregnated with an activating agent, and then it is directly activated without carbonization.

2.5.1.1. Physical (Thermal) Activation

Even all carbonization process of organic matters create porosity, they do not show their maximum potential of porosity; their pore volume and surface area are typically low without activation. Therefore, carbonized materials are activated with steam and CO_2 gases to achieve a better adsorption potential. After the carbonization step, the material is subjected to a heat treatment with steam or CO_2, or both gases at 1100-1250 K [19]. These gases react with C atoms and create porosity according to following equations:

$$C + CO_2 = 2\ CO \quad \text{.....(5)}$$

$$C + H_2O = CO + H_2 \quad \text{.....(6)}$$

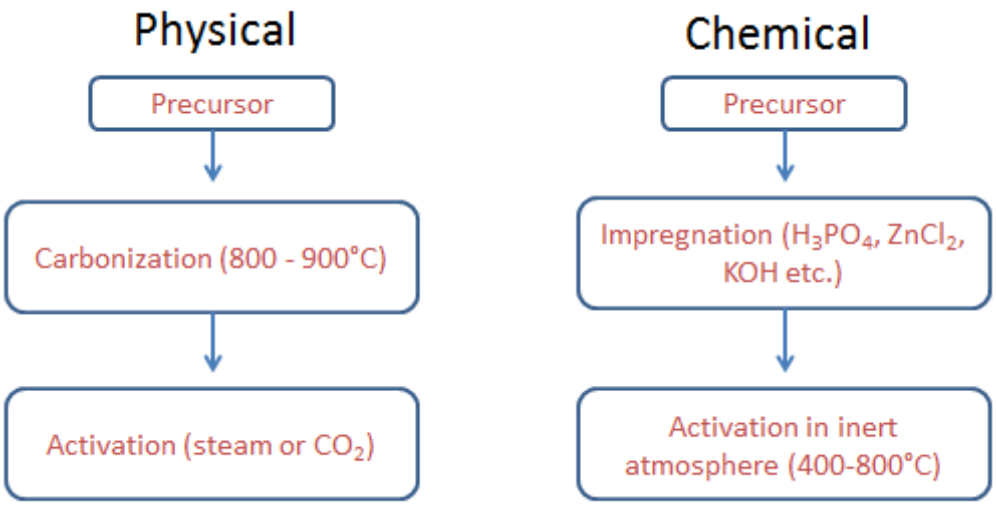

Figure 4. Physical and chemical activation routes for AC production.

In the process, the activating agents attack disorganized parts of the material, leaving the porous body after the treatment. The most important parameters are: precursor material, activating agent (steam or CO_2), final burn off, and presence of inorganic materials that catalyze the reactions.

2.5.1.2. Chemical Activation

Chemical activation of organic materials excludes the carbonization step; precursor is impregnated with an activating agent and heat treated in an inert atmosphere. The most widely used activating agents are H_3PO_4, KOH and $ZnCl_2$. The activation mechanisms for all agents are different; therefore, heat treatment temperature is chosen according to activating agent and corresponding activation mechanism.

Chemical activation of biomass depends on the degradation of the lignocellulosic structure. Impregnation ratio (mass of activating agent/mass of precursor) and activation temperature are the most important parameters for all activating agents. The choice of these parameters depends on the nature of the activation for a particular agent. The effect of impregnation ratio on porosity is similar for all activating agents; increasing it from 1 to higher values results in a change of porosity from mainly microporous (pores smaller than 2 nm) to mesoporous (pores larger than 2 nm, but smaller than 50 nm). However, activation temperature shows great discrepancies. $ZnCl_2$ and H_3PO_4 act as a dehydrating agent during the pyrolysis step and the activation occurs during pyrolysis, whereas KOH interacts with the precursor after pyrolysis. Pyrolysis of organic materials takes place at temperatures below 500 °C; therefore, activation temperature for $ZnCl_2$ and H_3PO_4 is typically lower (around 500 °C) than that for KOH (higher than 700 °C) [20]. $ZnCl_2$ activation mechanism and its effect on porosity of the resulting AC are studied by Caturla *et. al.* [21]. They used peach stones as precursor materials and studied various parameters that can affect the porosity such as impregnation

method and ratio, activation temperature and particle size. Increasing activation temperature from 500 °C to 800 °C resulted in a decrease in surface area. This reduction of surface area was attributed to volatilization of $ZnCl_2$ and pore shrinkage [22]. Furthermore, low values of impregnation ratio gives rise to narrow microporosity, while porosity widens as the impregnation ratio is increased, even mesoporous structure is achieved.

In a recent study, activation mechanisms of KOH and $ZnCl_2$ on wheat straw were investigated [23]. The mechanism of KOH activation is given as it includes intermediate products such as K_2O and K_2CO_3, and it is unevenly distributed. However, $ZnCl_2$, as a dehydrating agent, eliminates hydroxyl and carbonyl groups in the biopolymer and creates a thermoplastic phase during activation. Furthermore, $ZnCl_2$ has a melting point of 290 °C, evenly mixed with that phase in liquid state as seen in Figure 5. The mechanism of activation is described as follows: $ZnCl_2$ reacts with H_2O and produce zinc oxide chloride hydrate ($Zn_2OCl_2.2H_2O$). When temperature is raised, this compound decomposes to give $ZnCl_2$ gas, and gas diffusion in the thermoplastic phase creates porosity. A schematic for the process of the activation mechanisms for both KOH and $ZnCl_2$ are given in the Figure 5.

Further physical activation of $ZnCl_2$ AC's with CO_2 are reported in the literature [21, 24]. Burn off degree is given as the most important parameter affecting porosity, the rate of which is strongly influenced by heat treatment temperature. The temperature of partial gasification with CO_2 is typically higher (800 – 900 °C) than initial chemical activation temperature with $ZnCl_2$ (around 500 °C). This temperature increase influences the porosity of the material; in the initial stages of the treatment, (at low burn offs) the material goes through secondary carbonization process, see Figure 6. Therefore, surface area decreases and bulk density of the material increases at low burn offs (% burn off < 20%). After this drop of surface area, porosity starts to develop with the aid of CO_2 activating agent.

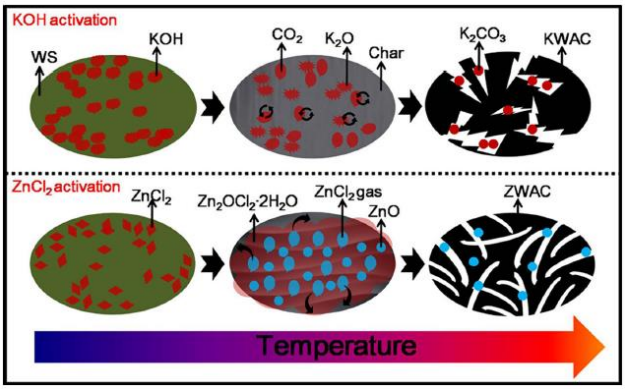

Figure 5. Schematics of $ZnCl_2$ and KOH activation mechanisms [23].

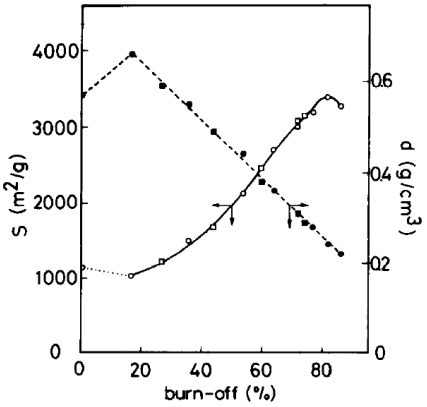

Figure 6. Evolution of surface area and density of the activated carbons with changing degrees of burn off [21].

2.5.2. Studies Based on Pine Cone as a Precursor to Activated Carbon Production

A wide variety of precursors were used for activated carbon production including coal, lignin, coconut shells, almond shells, sugar, sugar cane bagasse, waste tea, waste coffee beans and grounds, cotton stalks. In recent years, biomass waste usage as a precursor for the production of AC has gained importance to recycle the waste materials and reducing the costs. Pine cone, with extensive forests in

Mediterranean region [25] (35000 ha of Pinus pinea forest in Turkey), was also used for this purpose in the production of AC. Combustion behavior of pine cone was studied by Haykırı-Açma [26], and 9.4 wt.% moisture, 69 wt.% volatile matter, 20.9 wt.% fixed carbon and 0.7 wt.% ash was reported. The ash content of the pine cone is significantly smaller compared to that of other biomass materials in the study. In the article published by Duman *et. al.* [25], cone of Pinus pinea was activated with $ZnCl_2$ and H_3PO_4, and promising results were reported in the $ZnCl_2$ activated carbons as high as 1823 m^2/g surface areas. They also reported high volatile content for this precursor; yet, low ash content of the material makes it an appropriate precursor. Later, microwave treatment of $ZnCl_2$ impregnated pine cones were studied and 939 m^2/g BET surface area and 1.03 cm^3/g pore volume is achieved [27]. Pine cone based AC's were also studied in EDLC applications. In the article published by Karthikeyan *et. al.* [28], KOH activation was used for pine cone based activated carbons; 3950 m^2/g BET surface area and 2.395 cm^3/g pore volume was reported. They used these activated carbons to construct EDLC's with 1 M $LiPF_6$ dissolved in EC/DEC electrolyte, and as high as 61 Wh/kg energy density was achieved.

2.5.3. Characterization of Activated Carbon

AC characterization includes a wide variety of techniques such as gas adsorption, immersion calorimetry, SAXS, SANS, FTIR spectroscopy, Raman spectroscopy, SEM and TEM. Among these characterization methods, N_2 adsorption is used for the characterization of porosity and surface area, FTIR spectroscopy is used for determination of the surface functional groups, Raman spectroscopy is applied to analyze structural order, and SEM is conducted to characterize morphology of the particles and compositional analysis.

2.5.3.1. N_2 Adsorption

Adsorption is defined as increase in the concentration of a fluid at the close proximity of a surface. It results from interaction between the molecular forces of the surface and that of the fluid. As bonding is not completely satisfied at surface atoms, these are in a higher energy state. This creates an attractive force on the surface of the solids when they come into contact with fluids, causing surface excess concentration of the fluid.

This phenomenon has wide industrial applications areas. It includes liquid purification, gas separation, catalysis and so on. It is also used for the characterization of the surfaces [29, 30].

2.5.3.2. Adsorption Experiment

Figure 7 is the schematic drawing of the most widely used gas adsorption manometry. There are three valves and a pressure transducer used in the experiment. After the vacuum is broken, adsorptive is allowed to occupy the dosing volume. Then, temperature and pressure of the dosing volume is measured. After that, the adsorptive enters the adsorption bulb and adsorption takes place. After the equilibrium is attained, the pressure is measured again. The amount adsorbed is calculated from difference in the pressure.

All adsorption systems are dependent on amount adsorbed by the adsorbate, equilibrium pressure and temperature of the system. Therefore, the system can be expressed as:

$$\frac{x}{M} = f(p, T) \quad \text{.....(7)}$$

,where *x/M* is amount adsorbed per unit mass of adsorbate, *P* is pressure and *T* is temperature.

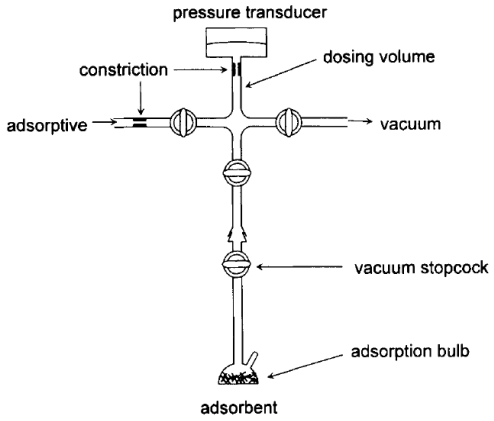

Figure 7. Schematic drawing of adsorption experiment setup [29].

If the adsorptive is a gas below its critical temperature, this equation can be written as:

$$\frac{x}{M} = f(p/p^0, T) \quad \text{.....(8)}$$

, where p is the equilibrium pressure and p^0 is the saturation pressure, the ratio p/p^0 is relative pressure.

Using above equation, adsorption can be expressed in three different ways: **adsorption isotherm** (variation of amount adsorbed with relative pressure at constant pressure), **adsorption isobar** (variation of amount adsorbed with temperature at constant pressure) and **adsorption isostere** (variation of temperature with pressure at constant amount adsorbed). However, this equilibrium is generally expressed as adsorption isotherm as it is the most convenient way.

2.5.3.3. Types of Adsorption Isotherms

Adsorption isotherms are categorized into 6 groups according to IUPAC classification [29], as given in Figure 8. The extent of adsorption and shape of the

isotherms are consequences of adsorbent-adsorbate interactions. Type 1 isotherm, with a sharp turning point and a broad plateau, is an indication of enhanced adsorbent-adsorbate interactions at low relative pressures. This isotherm type remarks microporous adsorbents with a low external area (area of roughness of the particles, excluding porosity). Type 2 isotherm specifies multilayer adsorption at high relative pressures, and beginning of the quasi-linear section, point B is accepted as the end of the monolayer adsorption. Type 3 and type 5 isotherms result from weak adsorbent-adsorbate interactions, and are not common. Type 4 isotherm is similar to type 2 isotherm except the high relative pressure hysteresis loop. This loop results from difference in the behavior when filling and emptying of mesopores by capillary condensation, therefore it is associated with mesoporous structure. Finally, isotherm 6 remarks layer by layer adsorption of uniform surfaces.

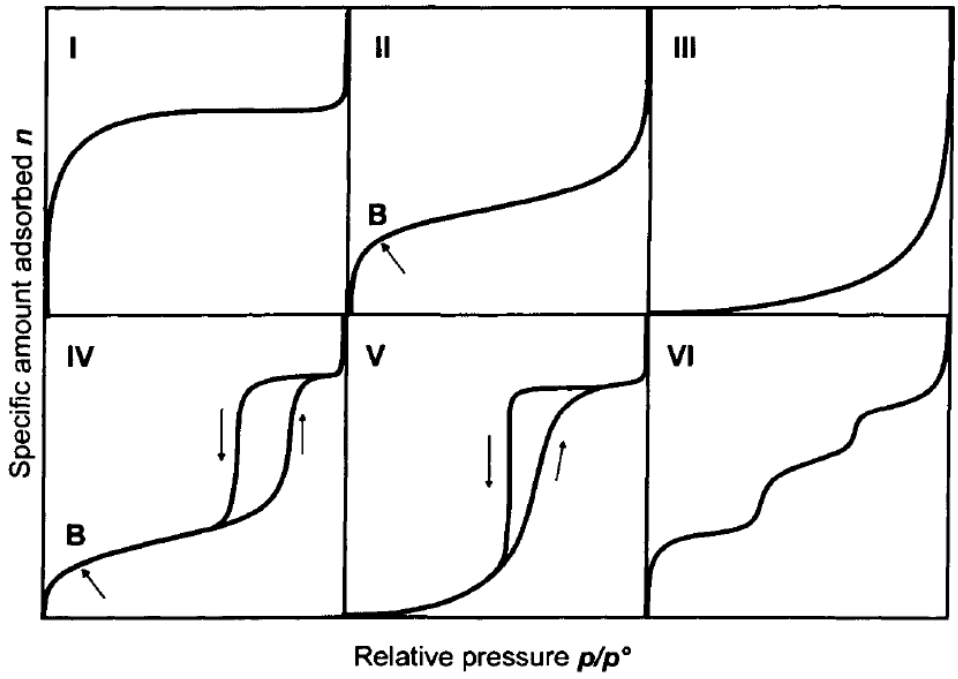

Figure 8. Types of adsorption isotherms [29].

2.5.3.4. Derivation of Surface Area and Pore Size Distribution from Adsorption Isotherms

Adsorption isotherms were extensively investigated and tried to be modeled by numerous researchers to obtain specific surface area, pore volume and pore size distribution. The earliest model to describe adsorption isotherm is proposed by Langmuir [31]. A kinetic approach is used in his model; rate of adsorption is assumed to be equal to rate of desorption at equilibrium. The derivation of his equation is based on the assumptions that surface is perfectly homogeneous and adsorption creates only monolayer at localized sites in which no lateral interaction of adsorbed species [30]. The equation he proposed was:

$$\frac{p/p^0}{\mathrm{n}} = \frac{1}{bn_m} + \frac{p/p^0}{n_m} \quad \text{.....(9)}$$

,where p/p^0 is the relative pressure, n is quantity of adsorbed gas per gram, b is a constant and n_m is the monolayer capacity.

After this influential work of Langmuir, many researchers tried to model adsorption process and solve the problem associated with Langmuir's oversimplified assumptions. Brunauer, Emmett and Teller proposed the most popular adsorption equation (BET), based on the assumptions similar to that of Langmuir [32]. They argued that adsorption does not only cover monolayer, rather it forms multilayers of adsorbed species as it progresses. Utilization of Langmuir concept (equating the rates of adsorption and desorption at equilibrium) for every adsorbed layer resulted in BET equation:

$$\frac{1}{v[\left(\frac{p^0}{p}\right)-1]} = \frac{c-1}{v_m c}\ \frac{p}{p^0} + \ \frac{1}{v_m c} \quad \text{.....(10)}$$

,where p/p^0 is relative pressure, V is volume adsorbed, c is a constant and V_m is the monolayer capacity. After calculating V_m, BET surface area can be derived from:

$$S_{BET} = N\, V_m\, a_m \quad \text{.....(11)}$$

,where N is Avogadro's number and a_m is the area occupied by single adsorbed molecule.

Although BET equation is successful in the interpretation of nonporous and macroporous surfaces, it should be used with care for heterogeneous surface materials. Because derivation of the BET equation is based on the assumption that surface is homogeneous, it can give incorrect evaluations in materials such as microporous AC's.

Studies after proposition of BET equation reveal that adsorption of gases on porous surfaces include several other phenomena besides multimolecular layer formation. One of them is capillary condensation, condensation of gases into wide pores (several diameters of the adsorbate, generally higher than 1 nm) with increasing relative pressure. The hysteresis in the high relative pressure part of adsorption isotherm is associated with this phenomenon, and frequently used pore size distribution determination method BJH (Barrett, Joyner and Holenda, after their names) is based on it. However, the use of BJH method is applicable only to mesoporous materials [29]. Another phenomenon in adsorption is put forward by Polanyi and modified by Dubinin, and it is named as volume filling of micropores. Due to the greater adsorption potential of the micropores, pore volume is occupied by the adsorbate, without forming the multilayer. Dubinin and Radushkevich derived an equation (DR equation) based on this theory, and it is still in use for the microporous adsorbents.

Since adsorption is a complicated process and all isotherm equations are based on some assumptions, their utilization must be conducted with care. In a paper published by Kaneko [33], use of BET equation in its classical relative pressure range (0.1-0.3), it is argued that BET model overestimates the surface area. The reason of overestimation is stated to be due to quasi-capillary condensation in wide micropores. They suggested to use more restricted relative pressure region to prevent calculated surface area increase. In another research, Centeno et al [34] reported increase in BET surface area with increasing pore width. Therefore,

surface area overestimation in BET model is a serious problem in dealing with microporous AC.

The application of DR equation has also its problems. Because it is based on volume filling of micropores, any other contribution to adsorption such as multilayer formation and capillary condensation is disregarded. Therefore, the adsorbent must be strictly microporous to use DR equation. Furthermore, N_2 adsorption is problematic in narrow micropores due to diffusion restrictions at 77 K. As a result, DR equation is generally applied to CO_2 adsorption isotherms for narrow micropore size AC's [35].

More recently, molecular modelling of adsorption gained importance for interpretation of the adsorption isotherms. Among them, density functional theory (DFT) based ones are particularly widely used. There are two different approaches in DFT models of adsorption: Non-local DFT (NLDFT) and Quenched solid DFT (QSDFT). Although detailed description of these models is beyond the scope of this study, some of their properties are mentioned. Both of them are capable of extracting surface area and pore size distribution for both microporous and mesoporous adsorbents. This property does not exist in any of the adsorption isotherm equations. A false gap in the pore size distribution around 1 nm arises in the NLDFT model; therefore, QSDFT method is preferred by numerous researchers [34].

2.5.3.2. Raman Spectroscopy

Raman spectroscopy makes use of inelastic scattering of light when exposed to a material. Most of the radiation is elastically scattered by light with the same wavelength. This is called as Rayleigh scattering. However, some of the incident radiation scatters inelastically, causing a difference in the energy states of the molecules. Raman spectroscopy uses this inelastically scattered light to achieve information about the vibrational states of the molecules.

Raman spectroscopy is a widely used tool for characterizing carbonaceous materials. The investigation of carbons using Raman scattering dates back to study of Tuinstra *et. al.* in 1969 [36]. A number of carbon materials, including single crystal and polycrystal graphites, AC and glassy carbon were used in this study. In the single crystal graphite, only one peak was observed at 1575 cm^{-1}, whereas another peak at 1355 cm^{-1} was found for other carbonaceous materials. It is argued that the intensity of the peak at 1355 cm^{-1} is inversely proportional to crystal size of the carbon; therefore, this peak is considered to be a measure of disorder and called D band. On the other hand, the peak at 1575 cm^{-1} is named as G band, and regarded as a measure of order.

2.5.3.3. FTIR Spectroscopy

Fourier transform infrared spectroscopy is a widely used technique to identify primarily organic materials. This technique is based on the absorption of infrared radiation by the molecules constituting the sample. Molecules have certain vibrational frequencies, depending on geometry of molecule and bonding. When the infrared radiations of entire range of frequencies strike to molecules, they absorb the radiations at certain frequencies that are in resonance with their vibrational frequencies. By this way, molecular identification can be accomplished as the absorbances only occur at the molecule-specific frequencies. However, not all of the molecules can be characterized by this technique. Since the absorption amplitude depends on the dipole moment of the molecule, the molecules that are not experiencing dipole moment change upon infrared radiation exposure cannot be identified by FTIR analysis [37].

FTIR investigation of carbon materials generally focuses on surface functional group characterization. Since carbons are black and they absorb most of the radiation, the assignment of surface functional groups is reported to be problematic [38]. Yet, numerous research groups used this technique; they generally evaluate

the results qualitatively, and utilized other techniques besides FTIR (such as Temperature Programmed Desorption and X-ray Photoelectron Spectroscopy) to precisely define the surface functional groups.

2.6. Effect of Porosity and Surface Area on Capacitance

Classical capacitance calculation states that surface area is proportional to capacitance, therefore to increase specific capacitance (F/g), the specific surface area (m^2/g) of the electrode active material must be enhanced. In studies relating surface area and capacitance, the results were found to be contradicting to this implication. In a paper published by Shi [39], specific capacitances of AC fibers and microbeads were plotted versus DFT specific surface area. The reason to use DFT area, rather than BET area, was reported as BET model overestimates the surface area. Surface area and capacitance were not linearly related in his findings as given in the Figure 9 (a). He suggested a model, assuming that electroadsorption properties of micropores and mesopores are different, total capacitance can be expressed as two portions:

$$C = C_{micro}S_{micro} + C_{meso}S_{meso} \quad \text{.....(12)}$$

Using this equation and plotting C/S_{meso} versus S_{micro}/S_{meso}, a linear relationship was found and the values for C_{micro} and C_{meso} are given for series of AC fibers and microbeads.

In a later work, Barbieri *et. al.* [40] analyzed the effect of surface areas and porosities of various carbonaceous materials in organic electrolytes. They reported a plateau in specific capacitance values for carbons having surface areas larger than 1200 m^2/g based on DFT, see Figure 9 (b). The model proposed by Shi was applied; however, C_{meso} values were found to be negative, which has no physical meaning. Furthermore, assuming totally different electrochemical behavior for pores larger than 2 nm was argued to be oversimplification. Reduction in

capacitance improvement was related to decrease in pore wall thickness as surface area and pore volume increases. As pore walls are getting thinner, the electric potential does not reach to zero. Therefore, surface area increase does not result in an enhancement in capacitance.

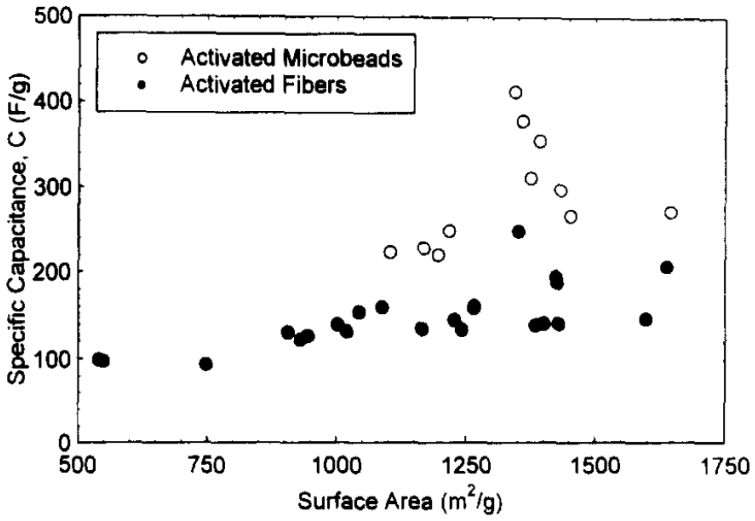

(a)

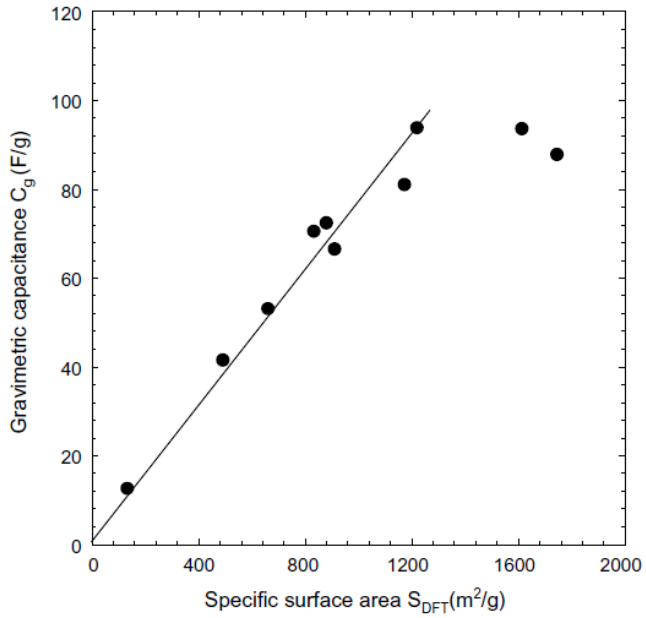

(b)

Figure 9. Specific surface area vs specific capacitance given in the papers published by a) Shi [39], b) Barbieri *et. al.* [40].

Obviously, charged species in the electrolyte cannot be treated as the point charges, since they have definite sizes. As a great portion of the porosity in carbons (especially in microporous ones) is smaller than 1 nm, part of the surface area created by the pores smaller than the ion size, cannot be used for the double layer capacitance. Actually, if all of the porosity is smaller than the ion size, capacitive current drops to zero; the ions are completely sieved. This logical assumption was illustrated by Eliad *et. al.* [41]. In this work, carbons with various pore sizes were used in different electrolytes. Cyclic voltammograms of double layer capacitors with two carbons (5.1 and 5.8 Å average pore sizes) and 3 electrolytes ($MgSO_4$, Li_2SO_4 and $MgCl_2$) are given in Figure 10. The CV of carbon with 5.8 Å pore size in $MgSO_4$ electrolyte is nearly rectangular (ideally rectangular for capacitive behavior), while the CV of carbon with 5.1 Å pore size has negligible capacitance; in other words, the ions are almost completely sieved in the latter case. Moreover, larger size bivalent cations and anions are also sieved; SO_4^{-2} and Mg^{+2} ions have small capacitance in $MgCl_2$ and Li_2SO_4 electrolytes.

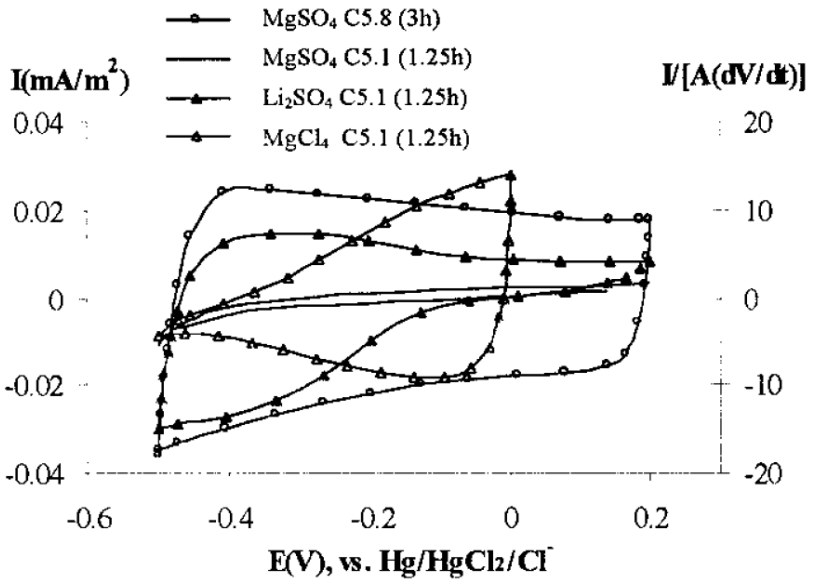

Figure 10. CV of carbons with 5.8 and 5.1 Å pore sizes, using 0.1 N $MgSO_4$, Li_2SO_4 and $MgCl_2$ electrolytes at a scan rate of 0.2 mV/s [41].

Having seen how the capacitive response delicately depends on the porous texture of a material, the question, then, arises: What must be the optimum pore size distribution and average pore size to achieve high capacitance values? The classical evaluation of the double layer points out that the ions enter the pores in their solvated states; therefore, pore size must be greater than solvated ion size. Otherwise, ions are inaccessible to pores, and carbons with high mesopore volumes have better specific capacitances [42]. Chmiola *et. al*., however, reported outstanding capacitance increase for carbons having average pore sizes smaller than 1 nm [43]. They normalized the capacitance by surface area, and found 40% capacitance reduction when average pore size got larger even surface area was increased by 60%. A three stage model was proposed to explain this behavior; in the first and second region, when pore size reduced to lower than twice of the solvated ion size, the normalized capacitance also decreased as a result of diminishing the usable surface area. In the third region, contrary to former arguments, normalized capacitance increased 100%, as seen in Figure 11. This finding was attributed to distortion of the solvation shells in such small pores and smaller distance to electrode surface.

The interaction between porous structure of carbonaceous materials and ion size of electrolytes were studied by Largeot *et. al.* [44] using ionic liquids. Because ionic liquids are solvent free electrolytes and no complications are introduced by the solvation shell in double layer, understanding pore-ion relationships is simpler than one in the organic or aqueous electrolytes. The results they obtained support the findings of Chmiola *et. al*.; the maximum normalized capacitance was found in the pore sizes below 1 nm. The normalized capacitance reached a maximum around 0.7 nm pore sizes as seen in Figure 12. Considering cation and anion sizes (0.76 and 0.79 nm, respectively), ion size must be close to pore size. Smaller pore sizes have inferior performance as a result of sieving effect, while larger pore sizes suffers from inefficient packing of ions due to size mismatch.

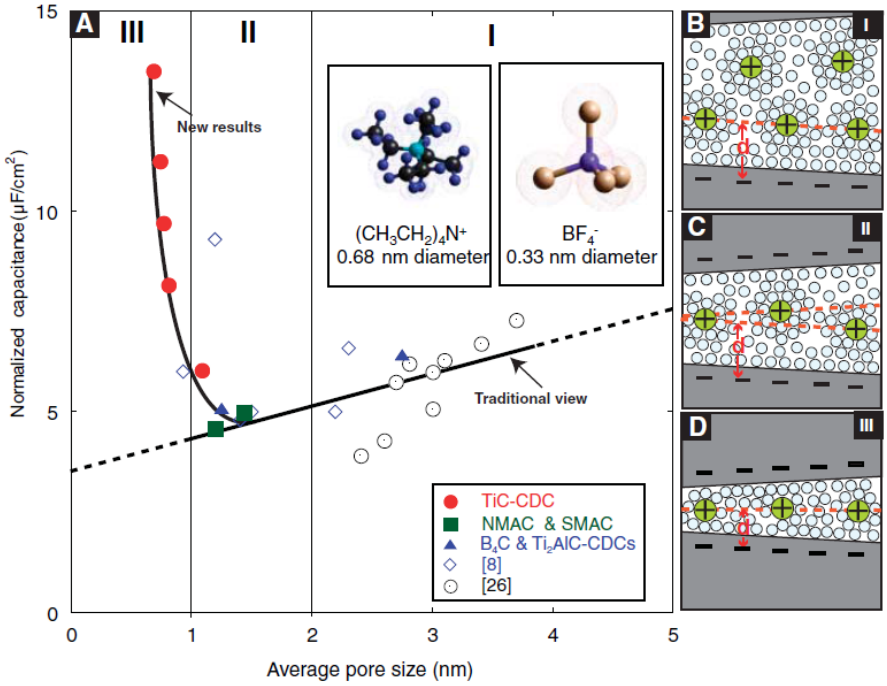

Figure 11. A three stage model of normalized capacitance as a function of average pore size proposed in [43].

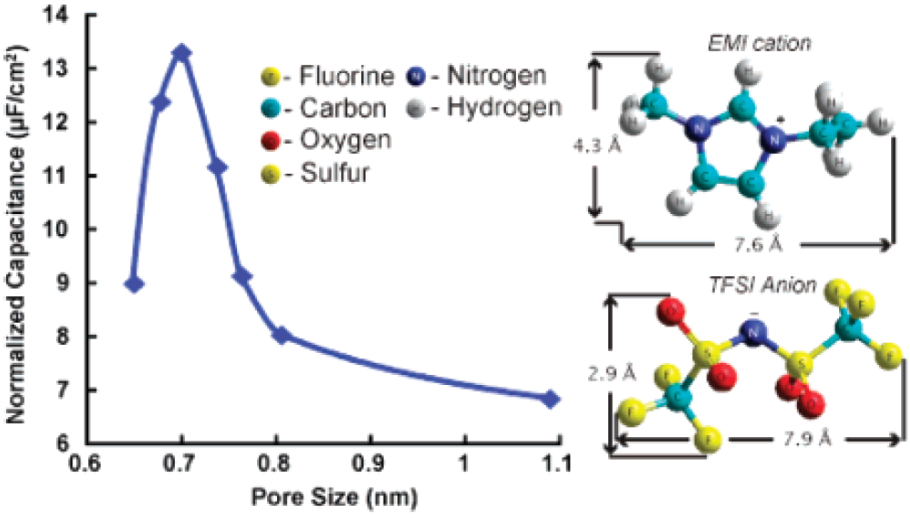

Figure 12. Normalized capacitance (by specific surface area) vs. pore size of the carbide derived carbonaceous materials with EMI-TFSI ionic liquid [44].

The problem associated with pore-ion interaction was further analyzed using organic electrolyte (1.5 M TEA BF_4 in acetonitrile) in three electrode cell configuration [45]. The difference between solvated and bare ion sizes were taken into account: 1.30 - 0.67 nm for TEA^+, and 1.16 – 0.48 nm for BF_4^- ions for solvated and bare ion sizes, respectively. The capacitance values were calculated for both negative and positive electrodes with the aid of three electrode cell. These values had a maximum around 0.7-0.8 nm pore sizes, being smaller for the anion (Figure 13). Since the pore sizes that give maximum specific capacitance were substantially smaller than the solvated ion sizes, they had a conclusion that ions form double layer at small micropores as in their desolvated states.

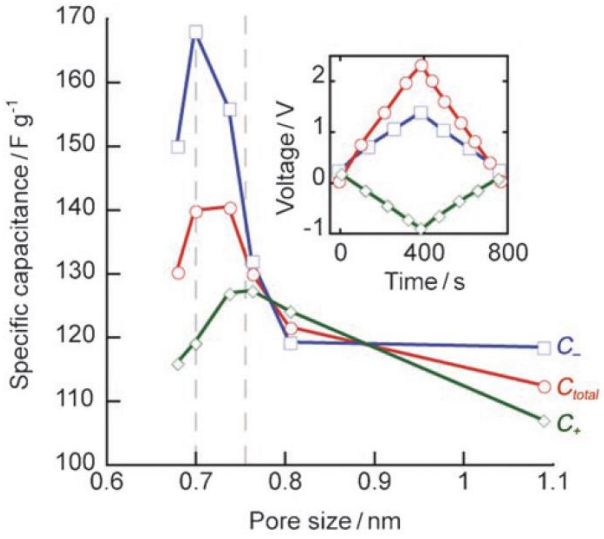

Figure 13. Specific capacitance change as pore size changes for positive electrode, negative electrode and total. [45].

Effect of textural characteristics of carbons on capacitance is not restricted to average pore size alone. The capacitive performance of carbons can also be affected by development of porosity. In the study of Mysyk *et. al.* [46], a saturation phenomenon was observed when the porosity was inadequately

developed. When cyclic voltammetry was applied to two carbons with different porosity (Figure 14, a), one with narrow pore size distribution and smaller surface area (pitch based, named as PC) did not show quasi-rectangular CV shape and a drop in the capacitive current was observed, while the drop was not seen in the carbon with wide pore size (viscose based, named as VC). The reason of this current decrease at high voltages was attributed to complete coverage of surface before reaching electrolyte decomposition voltage. Thus, matching average pore size to ion size is not enough to achieve optimum capacitive performance, unless porosity is sufficiently developed.

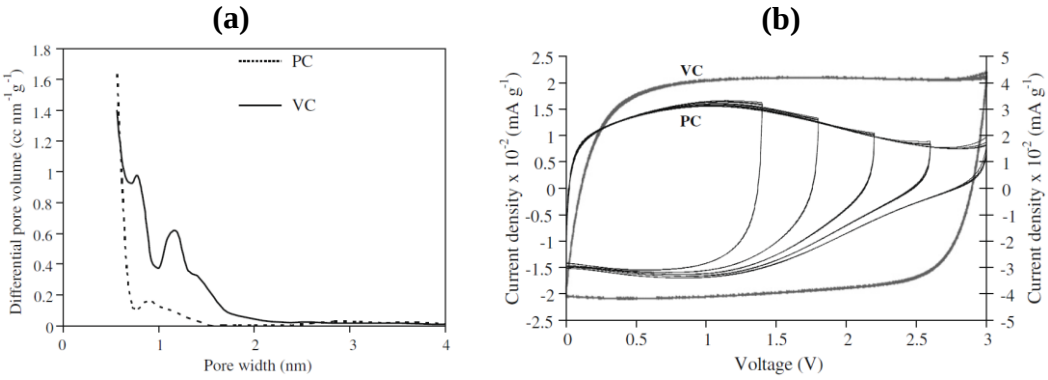

Figure 14. Pore size distributions of two carbons (a), and their cyclic voltammograms (b) with 1.5 M TEA BF_4 in acetonitrile at 5 mV/s [46].

After the first investigation of the porosity saturation phenomenon, effect of ion size on saturation was studied using organic electrolytes with several salts [47]. Due to the bigger size of the cations compared with anions, capacitance was argued to be dependent on cation size. Therefore, tetraalkyl ammonium ions with different lengths were used. Small sized cations did not reveal porosity saturation, while this behavior was observed for bigger ones. Moreover, the beginning point of capacitive current reduction dropped to lower voltages when cations got bulkier.

Surface area used by bigger sized cations was larger, so that the space provided for double layer formation was quickly spent as voltage increases.

Evaluation of porous structure on capacitance brought about new interpretations in the study of Ania *et. al.* [48]. They reported similar specific capacitance values for two carbons with completely different porosity characteristics; one was microporous and had low surface area, and the other was micro + mesoporous and had high surface area. Normalization of the capacitances by the surface area resulted in two times higher values for microporous carbon with narrow pore size and lower surface area. This result was explained as a consequence of cation distortion when the double layer is formed in narrow micropores. The cations were suggested to enter the pores in distorted geometries under the effect of polarization; thus, surface area available for cation electroadsorption is more than calculations based on rigid cation sizes (0.68 nm for TEA^+) for narrow pore size carbons, see Figure 15. On the other hand, carbons with wide pore size underuse the pore volume as a result of inefficient packing. Moreover, this packing condition gives rise to increase in the distance between electrode surface and the ion, deteriorating capacitance values.

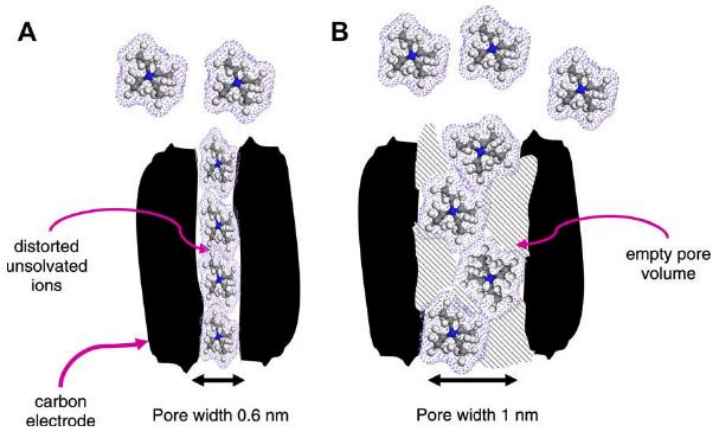

Figure 15. Pore size effect on the pore ion interaction A: pore width smaller than the size of the rigid ion size B larger pore [48].

2.7. Studies Based on $ZnCl_2$ AC's as EDLC Electrodes

Although various chemical activating agents are available for AC production, KOH is the most widely used one in EDLC applications and it is followed by $ZnCl_2$ [49]. In particular, $ZnCl_2$ activated carbons were studied as EDLC electrode materials by several researchers. Subramanian *et. al.* [50] derived AC's from banana fiber using both $ZnCl_2$ and KOH activating agents. $ZnCl_2$ AC's had a superior performance in neutral aqueous electrolyte (1 M Na_2SO_4), with 1097 m^2/g specific surface area and 74 F/g specific capacitance at a current density of 500 mA/g. Rufford *et. al.* [51] also used aqueous electrolyte for EDLC study on $ZnCl_2$ AC's (1 M H_2SO_4). They derived AC's from waste coffee beans, with 1 impregnation ratio of $ZnCl_2$ at 900 °C. The specific surface area and pore volume of the AC were 1019 m^2/g and 0.48 cm^3/g, respectively. Specific capacitance was reported to be 368 F/g, and such a high value was attributed to pseudo-faradic contributions from carbonyl-quinone and nitrogen functional groups. The same research group published two other articles on EDLC construction of $ZnCl_2$ AC's [22, 52]. In the first article, sugar cane bagasse was used as precursor and 1 M H_2SO_4 was used as electrolyte, while in the second article waste coffee grounds and 1 M TEA BF_4 in acetonitrile were used as precursor and electrolyte. In the first paper, precursors were impregnated with $ZnCl_2$ with impregnation ratios of 1, 2 and 3.5. Heat treatment temperatures were 750 and 900 °C, and it is stressed that although $ZnCl_2$ activation is more effective in lower temperatures, the resistivity of low temperature treated AC limits its use in EDLC applications. With increasing impregnation ratio from 1 to 3.5, BET specific surface area rose from 1155 to 1788 m^2/g, so did mesopore volume, from 0.26 to 1.55 cm^3/g. Specific capacitances were reported in this study to be nearly 300 F/g. Capacitance retention at high current densities were superior in the carbons having larger mesopore volumes. In the second paper, about 100 F/g specific capacitance and 16.5 Wh/kg energy density was found at high current densities. The impedance behaviors of $ZnCl_2$ AC's with several porous texture characteristics gave the conclusion that ion transport is faster in mesopores.

In this study, $ZnCl_2$ AC's are produced and used in EDLC fabrication. One of the key factors in EDLC applications is electrical conductivity of the active material. Although the treatment temperature dependence of conductivity of $ZnCl_2$ AC's was briefly explained in literature, the systematic investigation and reasons of conductivity dependence is newly introduced in this study. Furthermore, although use of LA 135 binder was studied in EDLC, LA 132 binder is firstly utilized in EDLC to the best of my knowledge.

CHAPTER 3

EXPERIMENTAL PROCEDURE

The experimental procedure is viewed in three sections. The first one is the methods used in the production of AC's. The second section focuses on the structural and chemical characterization of the AC's, and the last one is about electrode preparation, cell assembly and electrochemical characterization of the EDLC's.

3.1. Preparation of Activated Carbons

Preparation route of AC's are divided in two steps: two samples were obtained by chemical activation with $ZnCl_2$, and these two samples were heat treated further in two different atmospheres.

3.1.1. Preparation of Only $ZnCl_2$ Activated Carbons

Pine cones (pinus pinea, given in figure 16) were collected from Mediterranean region of Turkey, and they were held in ethyl acetate for two days to remove the resin stuck from it. After removal of the resin layer, pine cone was dried in open atmosphere for several days. Dried cones were crushed and ball milled at 200 rpm for 15 minutes, and sieved to 50 mesh. Then, 8 grams of the precursor was weighted to be impregnated with $ZnCl_2$ (Sigma-Aldrich, purity > 98%) aqueous solution. Impregnation ratio, one of the most important parameters in the production of chemically AC's, is given by:

$$\boldsymbol{Impregnation\ Ratio\ (IR)} = \frac{\textbf{Weight of } \boldsymbol{ZnCl_2}}{\textbf{Weight of pine cone}} \quad \text{.....(13)}$$

$ZnCl_2$ aqueous solutions were prepared in 20-25 ml of deionized water with 8 and 32 grams of $ZnCl_2$, used for 1 and 4 impregnation ratio samples, respectively. After mixing the precursor with the $ZnCl_2$ solutions, the impregnation step was conducted at 110 °C. As a first step, water was evaporated on a hot plate and the mixture was homogenized by magnetic stirrer. In this stage, swelling of the particles and color change to black were observed, especially for 4 *IR* sample. Then, after evaporation was complete, the samples were put in a drying oven and kept overnight.

The activation step was carried out in a horizontal tube furnace, under N_2 gas at a flow rate of 0.2 l/min and a heating rate of 20 °C/min. Before heating the samples, the furnace was kept at 5 l/min flow rate N_2 gas for 10 minutes to remove the air. The activation temperature and time were kept at 500 °C and 2 hours. After the activation step was completed, samples were washed with 1 M HCl and hot distilled water, until a pH value of 6.5-7 was reached. The samples were designated as 15 and 45 as given in Table 1, indicating impregnation ratio in the first number and heat treatment temperature in the second number.

Figure 16. Photos of Pinus pinea used for AC production.

Table 1. Experimental parameters for only $ZnCl_2$ activated samples**.**

	IR	Act. Temp. (°C)	Act. Time (h)
15	1	500	2
45	4	500	2

3.1.2. Preparation of Vacuum Treated Activated Carbons

Vacuum heat treatment was applied to $ZnCl_2$ AC's in a vacuum furnace with a rotary pump and a diffusion pump connected to it. 1 gram of carbon was placed in the furnace. After samples were placed, first rotary pump was activated and pressure dropped to 10^{-2} mbars. Then, diffusion pump was put on, and the pressure dropped further to 10^{-6} mbars. Heating rate was 5 °C/min for both activated carbons. Treatment temperature and time were kept constant at 950 °C and 5 hours. About 10% weight was lost in the treatment for both carbons. The samples were designated as 15-vac and 45-vac.

3.1.3. Preparation of CO_2 Treated Activated Carbons

CO_2 treatment of $ZnCl_2$ AC's were conducted at a flow rate of 0.5 l/min CO_2 gas, at 800 and 900 °C. Heating rate was 5 °C/min. Activation times were 12 and 36 hours for 800 °C and 5 hours for 900 °C. CO_2 treated samples were designated as 15-c12, 15-c36, 45-c12, 45-c36 for 800 °C, indicating activation time, and 15-c900 and 45-c900 for 900 °C, remarking activation temperature (see Table 2).

3.2. Characterization of Activated Carbons

Electrical conductivity measurement, scanning electron microscopy, N_2 adsorption, FTIR spectroscopy, and Raman spectroscopy techniques were applied

to AC materials to analyze their morphology, porosity, functional groups and structural order.

Table 2. Experimental parameters of CO_2 treated samples.

Sample Code	IR	CO_2 Act. temp.	CO_2 Act. time
15	1	-	-
15-c12	1	800	12
15-c36	1	800	36
15-c900	1	900	5
45	4	-	-
45-c12	4	800	12
45-c36	4	800	36
45-c900	4	900	5

3.2.1. Electrical Conductivity Measurement

AC's were ball milled at 25 Hz frequency for 10 minutes to achieve smaller size particles and homogeneous particle size distribution, in order to reduce contact resistance. Measurements were done in directly powdered AC's, without any additive. An apparatus was designed for direct electrical conductivity measurement from powders. Two brass plugs, in between the powder to be measured, were fixed with clips, and the region where powder resides was isolated with a PEEK cylinder as shown in Figure 17. The applied force in the electrical conductivity measurements of AC's has influence on the results, therefore the height of the AC powder was kept around 1 mm to ensure the force applied by clips did not change considerably. After this apparatus was assembled, electrical conductivities of AC's were measured in Modulab MTS Solartron Analytical for the module suitable for highly conductive materials. Conductivity was measured in DC current at a constant voltage of 5 mV for 10 minutes. Using average values of voltage and current, resistance was calculated according to Ohm's law.

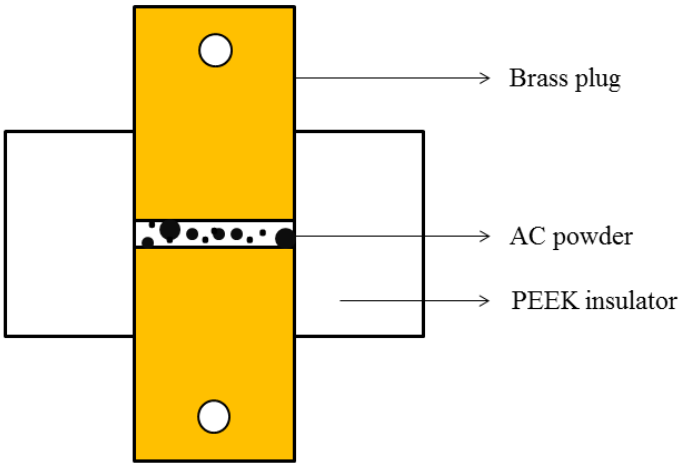

Figure 17. Cross sectional view of electrical conductivity measurement apparatus.

3.2.2. Scanning Electron Microscopy (SEM)

Powdered pine cone was coated with gold before SEM investigation (FESEM, Nova NanoSEM 430), to eliminate charging problem as a result of low electronic conductivity of the material. AC's were investigated as produced. Powders were stuck to carbon tape on aluminum holders. SEM micrographs at various magnifications (500X, 1000X, 2000X, 8000X) were taken to observe morphology of the particles. Accelerating voltage of 20 kV and spot size of 3.5 were used for electron micrographs. Chemical composition analyses were obtained with the use of Energy Dispersive Spectroscopy (EDS). Accelerating voltage was increased to 30 kV in the EDS to increase dead time. To prevent contributions from carbon tape, beam was focused on larger particles at high magnification (around 10000X). Since EDS investigation of carbon was problematic due to its low atomic number, the spectra was used for comparative purposes.

3.2.3. Other Characterization Techniques

N_2 adsorption was applied to AC's in Autosorb-6 at 77 K. Before the measurement, samples were kept in vacuum at 200 °C for 3 hours, in order to

remove the gases adsorbed onto them (degassing). Surface area and pore size distribution were calculated in Quantachrome Autosorb software. Pore size distribution calculation was conducted using QSDFT equilibrium model for N_2 at 77 K on carbon for slit pore geometry, given in the software. Average pore size was based on weighted average of cumulative surface area. Raman spectroscopy was applied using Renishaw inVia Raman spectrometer with a 532 nm wavelength laser. Deconvolution of the peaks was conducted using 2 Lorentzian peaks for D and G bands. FTIR spectroscopy was applied using Perkin Elmer Frontier spectrometer in attenuated total reflectance (ATR) mode. Background was subtracted before spectrum was obtained. Analyses were performed in directly to AC's, without any addition.

3.3. Electrochemical Characterization

Produced AC's were ball milled at 25 Hz for 10 minutes to achieve uniform particle size distribution and smaller particle size. After ball milling, 0.3 g of AC was mixed with 0.0375 g carbon black as a conductive additive (Super C65), and 1.5-2.0 ml of distilled water. This mixture was ball milled again at 25 Hz for 10 minutes to effectively distribute the conductive additive. Two commercial binders were used in this study: PSBR 100 and LA 132. They were both aqueous binders having 15 % solid content. The structure of PSBR 100 was composed of styrene butadiene rubber (SBR) and carboxyl methyl cellulose (CMC), while that of LA132 was polyacrylic latex. 0.25 g of either PSBR 100 or LA 132 was dripped into the mixture and ball milled again to distribute the binder. Frequency was kept at 20 Hz and milling time was reduced to 1 minute, not to deteriorate the properties of binder. Final proportion was 80 % active material (activated carbon), 10 % conductive additive (carbon black) and 10 % binder (PSBR 100 and LA 132). This slurry was coated on aluminum and nickel foils (LA 132 binder to aluminum foil and PSBR 100 binder to nickel foil) with doctor blade. This was a delicate process; unless the viscosity of the slurry was optimum, sticking problem

to foil surface was observed. The viscosity of the mixture was completely different for different active materials; porosity of the activated carbons had a remarkable effect on viscosity of the final slurry. Therefore, different water contents were tried to minimize the sticking problem. Then, the foils were kept at room temperature to dry. After completely dried, electrodes were cut into 18 mm stamps from this foil. Stamps were put in a vacuum oven and left overnight at 80 °C and 20 mbars. Dried stamps were put in glove box immediately.

Button type cells were constructed in a glove box, having H_2O and O_2 content of less than 0.1 ppm. Glass fiber separators were used in cell construction. TEA BF_4 (Aldrich, 99% pure) and TBA PF_6 (Aldrich) salts were used in this study in the electrolyte. The salts were kept in vacuum oven at 110 °C and 20 mbars before taken into the glove box. They were dissolved in acetonitrile (Merck, max. H_2O content<0.005 ppm) in the glove box to obtain 1 M TEA BF_4 and 0.3 M TBA PF_6 in acetonitrile. Two electrode cells were used in this study.

Three electrochemical tests were applied to cells; cyclic voltammetry (CV), galvanostatic charge and discharge (GCD), and electrochemical impedance spectroscopy (EIS). CV was conducted at 10, 30, and 50 mV/s scan rates up to 2.7 V. The 20^{th} cycle was given in all figures, and used in capacitance calculations. The reason of giving 20^{th} cycle was that overestimated values can be found in the former cycles [60]. GCD was applied in three currents: 2 mA, 5 mA and 15 mA up to 2.7 volts. The 10^{th} charge-discharge curve was given in the figures, and discharge curves were used for the capacitance calculations. EIS was applied at frequencies between 100 kHz and 10 mHz, with 10 mV sine wave.

Capacitance was calculated in two ways: from the area under the cyclic voltammograms, and from the slope of the discharge curves. Capacitance calculation from the area under voltammograms was based on the equation 14, where C is capacitance in Farads, I is current in amperes, v is scan rate in V/s. To get the specific capacitance (F/g) in single electrode, this value was divided by total active mass of the electrodes, and multiplied by 4, for the assumption that two

capacitors are connected in series and half of the total active mass in single electrode.

$$\boldsymbol{C} = \frac{\int \boldsymbol{I(V)dV}}{\mathbf{2Vv}} \text{.....(14)}$$

Capacitance was calculated from galvanostatic charge-discharge experiments by the following formula;

$$\boldsymbol{C} = \frac{\mathbf{I}}{\frac{\boldsymbol{dV}}{\boldsymbol{dt}}} \text{.....(15)}$$

Assuming linear voltage profile, the slope was calculated from discharge curve by line fitting. The normalization procedure was the same as applied in the calculations in cyclic voltammetry. Specific capacitances given in the results and discussion part were calculated from voltammograms, while Ragone plots were derived from discharge curves, omitting the IR drops.

CHAPTER 4

RESULTS AND DISCUSSION

4.1. Characterization of Activated Carbons

4.1.1. N_2 Adsorption at 77 K

Determination method of surface area and pore size distribution of activated carbon has been a subject of controversy. Although BET model is widely used for surface area calculation, it overestimates surface area, especially when used in the relative pressure range of 0.05-0.3 for microporous solids. Kaneko *et. al.* [33] reported that restriction of the relative pressure range to lower relative pressures gives rise to more realistic results of BET surface area when applied to microporous carbons. Therefore, relative pressure range of 0.01-0.1 is used in this study for BET surface area.

Among various methods to evaluate pore size distribution of activated carbons having both micro and mesoporosity, DFT methods are considered to be the most reliable. NLDFT and QSDFT methods are both used in various researches; however, NLDFT gives a false gap around 1 nm [34]. Therefore, QSDFT method is used for analyzing pore size distribution.

Figure 18 represents adsorption isotherms of produced activated carbons for N_2 at 77 K (a and b) and their pore size distributions (c and d). According to BDDT classification [53], samples 15, 15-vac, 15-c12, 15-c36 and 15-c900 have type 1 isotherm characteristic of microporous adsorbents, while samples 45, 45-vac, 45-c12, 45-c36, and 45-c900 show type 1-4 hybrid isotherm shape, indicating mesoporosity. Consistent with previous studies [54,55], impregnation ratio has a quite pronounced effect on pore structure; 1 impregnation ratio samples are mainly microporous, while 4 impregnation ratio ones have a considerable amount of

mesoporosity along with microporosity as a result of pore widening. Furthermore, both post treatments also affect porosity; although they do not change the type of the isotherm, textural properties greatly differ with treatment time and temperature. There is no further activation in vacuum treatment since there is no activating agent in the environment. In vacuum treatment, pore structure changes as a result of high temperature exposure; porosity shrinks to lower sizes for both activated carbons. The effect of porosity shrinkage is much more pronounced for 4 impregnation ratio sample, with a mesoporous volume reduction to less than one third of its value for sample 45. Besides, micropore size gets smaller after treatment, resulting in disappearance of the peaks around 1 nm. However, this does not have a dramatic impact on micropore volume especially for sample 15. Therefore, micropore volume and surface area can considerably be preserved while narrowing the pore size by high temperature vacuum treatment for microporous activated carbons.

The behavior of CO_2 treated samples with low burn off degrees are found to be similar to vacuum treated ones. Burn off degree reveals the extent of activation, and it has a remarkable influence on surface area and pore volume creation. Both micropore and mesopore volume of sample 45 decrease when CO_2 treated; greater effect is seen in the mesopores as found in sample 45-vac. When the burn off degree increases, development of mesoporosity is evident as seen in samples 45-c36 and 45-c900. However, CO_2 treated samples cannot reach the initial mesopore volume and surface area of sample 45. On the other hand, sample 15 develops both surface area and pore volume as a result of high burn off degree CO_2 treatment in samples 15-c36 and 15-c900, while porosity narrows down and pore volume decreases in the low burn off treatment as seen in Table 3.

This porous structure difference with the extent of CO_2 activation can be ascribed to competition between porosity shrinkage and physical activation by CO_2. As a result of structural reorganization, activated carbons densifies when heat treated at a temperature higher than activation temperature, therefore pore structure

collapses. However, if CO_2 activation proceeds, this effect is eliminated and physical activation with CO_2 dominates the textural properties.

Although BET surface area calculations are restricted to 0.01-0.1 relative pressure range, the S_{BET} values are substantially greater than values given by DFT. As a more reliable assessment, values given by DFT calculations are used in the electrochemical characterization.

4.1.2. FTIR Spectroscopy

Surface functional groups on activated carbon greatly alter the electrochemical response when used in electrochemical capacitors. Their most important effects are reducing the conductivity of activated carbons and pseudocapacitance. To analyze them, IR spectroscopy, a widely used technique for qualitative evaluation of surface functional groups of carbon materials, is applied and given in Figure 19.

In the spectra, all the specimens have broad absorption bands around 1730, 1240, 1150 and 1080 cm^{-1}. Additionally, samples 15 and 45 have adsorption bands at nearly 1580, 875, 800 and 750 cm^{-1}. The intensities of these bands are greater on sample 45, and after the heat treatment applied to them, intensities of all the bands are greatly reduced. Moreover, 1580, 800 and 750 cm^{-1} bands completely disappear in both vacuum and CO_2 treated samples.

Since carbons absorb most of the radiation, and also the FTIR assignments of different functional groups are very close to one another, complex bands of the spectra should be interpreted with caution. The band around 1730 cm^{-1} is ascribed to C=O stretching vibrations of carbonyl groups, carboxylic acids and anhydrides, and lactones [56]. 1580 cm^{-1} band is associated with C=C stretching vibration in aromatic rings and quinones [57, 58]. C-O stretching mode of carboxylic acids and O-H bending mode are responsible for 1240 and 1150 cm^{-1} bands, respectively

[59, 60]. Finally, C-H out of plane vibration gives rise to 875, 800 and 750 cm^{-1} peaks [61].

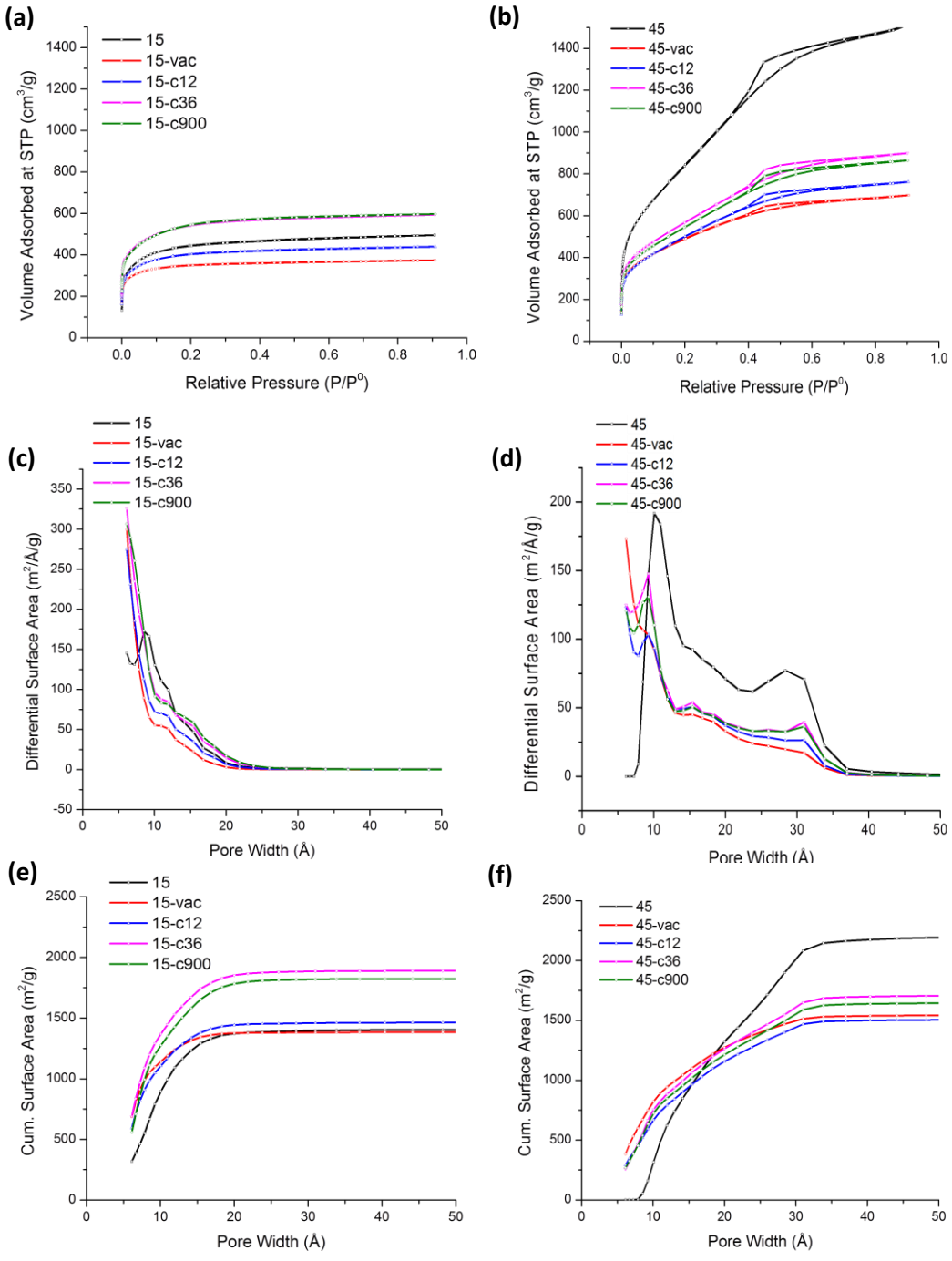

Figure 18. Adsorption isotherms (a and b), pore size distributions (c and d) and cumulative surface areas (e and f) of activated carbons.

Table 3. Surface area, pore volume and burn off degree of activated carbons.

	S_{BET} (m^2/g)	S_{DFT} (m^2/g)	S_{mic} (m^2/g)	S_{meso} (m^2/g)	V_{mic} (cm^3/g)	V_{meso} (cm^3/g)	L_0 (nm)	Burn off %
15	1666	1407	1373	32	0.65	0.05	1.03	-
15-vac	1329	1386	1376	9	0.52	0.01	0.81	-
15-c12	1513	1465	1444	20	0.59	0.03	0.89	14
15-c36	2007	1891	1853	37	0.8	0.04	0.93	28
15-c900	2001	1825	1784	40	0.8	0.05	0.96	34
45	2771	2218	1323	870	0.9	1.22	2.0	-
45-vac	1683	1549	1275	267	0.62	0.37	1.33	-
45-c12	1692	1512	1157	347	0.61	0.47	1.49	15
45- c36	1919	1714	1263	442	0.66	0.63	1.55	30
45-c900	1839	1652	1214	430	0.64	0.59	1.55	36

The reduction in intensity of the bands, even their disappearance, is a consequence of decreasing the surface functional group content of the activated carbons after heat treatment. However, the size of aromatic ring structure increases as the heat treatment temperature is enhanced. The disappearance of the 1580 cm^{-1} band of the vacuum and CO_2 heat treated samples does not result from the lower size of the aromatic ring clusters, rather it is due to the dipole moment increase of aromatic ring vibrations with the presence of surface oxygen atoms [56]. Consequently, surface functional groups of the activated carbons effectively removed via high temperature vacuum and CO_2 heat treatments.

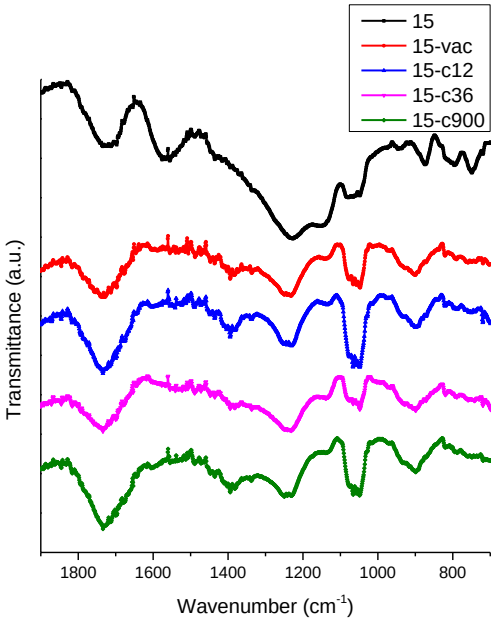

(a)

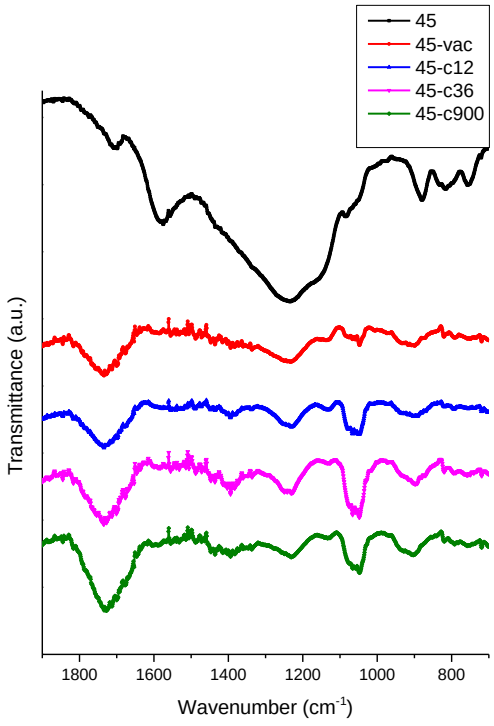

(b)

Figure 19. FTIR spectra of activated carbons, (a) 1 impregnation ratio, (b), 4 impregnation ratio

4.1.3. Raman Spectroscopy

Figures 20 and 21 display the Raman spectra of activated carbons, indicating characteristics of disordered carbon materials. They constitute a broad D band and a relatively sharp G band. G band is typically interpreted as a measure of order, whereas D band is considered to reflect disorder. The origin of G band is E_{2g} vibration mode of sp^2 bonded carbon atoms. The D band is associated with A_{1g} breathing mode, which is not allowed in single crystal graphite, only possible with the presence of disorder. Therefore, Tuinstra and Koenig offered I(D)/I(G) ratio as a parameter to assess the order of carbon materials, being inversely proportional to crystallite size [36]. In a later work, Ferrari and Robertson proposed a three stage model according to amorphization of carbon materials, from single crystal graphite to tetrahedral amorphous carbon with 100 % sp^3 bonding. They argued the intensity of the D band is associated with the existence of six folded rings, which increases with the increase of sp^2 bonded cluster size [62]. Therefore, I (D)/ I (G) ratio increases with more ordered structure with greater sp^2 cluster area in the stage 2 of their model, from amorphous carbon to nanocrystalline graphite.

Another parameter to be considered to determine structural order of activated carbons using Raman spectroscopy is full width at half maximum (FWHM) of the D band. Narrowing down of the D band is linked to the enhancement of the structural order, due to the reduction of contributions from distribution of amorphous carbon structures within ordered structure [61] and bond angle disorder [63].

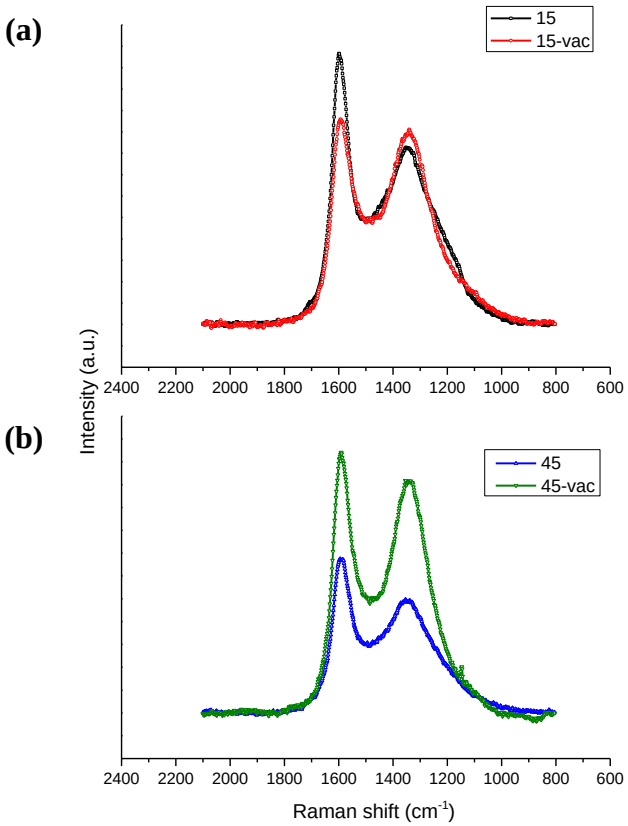

Figure 20. Raman spectra of only $ZnCl_2$ activated and vacuum treated activated carbons, (a) 1 impregnation ratio, (b), 4 impregnation ratio.

Table 4 represents the intensity ratios of D and G bands, and FWHM of the D band of the activated carbons. As a previous study stated [59] the effect of porosity on the order of the activated carbon is not pronounced; slight increase in intensity ratio and decrease in FWHM of D band is attributed to difficulty in representing these spectra with 2 peak fits and experimental errors. The stronger effect is seen on the heat treatment; I(D)/I(G) ratio increases and FWHM of D band decreases significantly as heat treatment temperature or time increases. This consequence

clearly shows that vacuum and CO_2 heat treated samples have much larger sp^2 domains and more ordered structure.

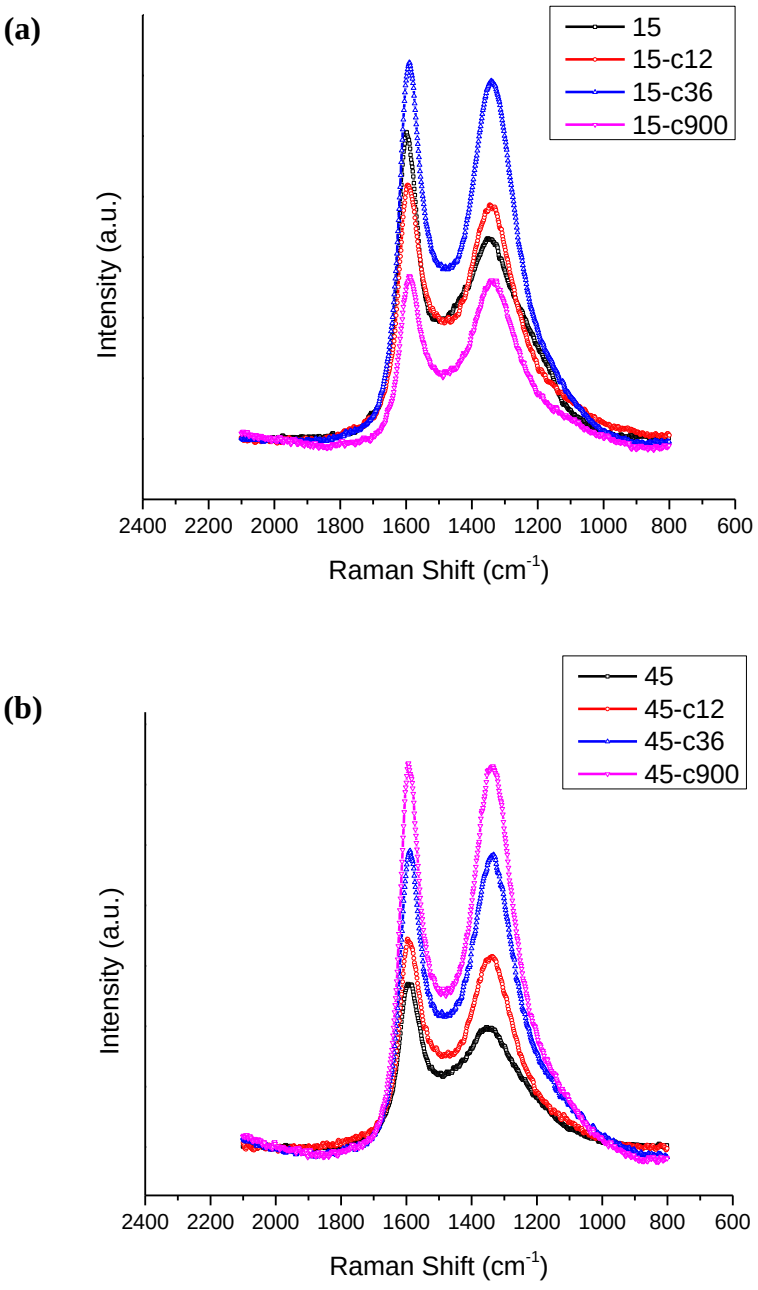

Figure 21. Raman spectra of only $ZnCl_2$ treated and CO_2 treated activated carbons, (a), 1 impregnation ratio, (b), 4 impregnation ratio.

Table 4. I(D)/I(G) ratio and FWHM of D band, calculated by 2 Lorentzian peak fits.

	I(D)/I(G)	FWHM (D) cm^{-1}
15	0.72	262.2
15-c12	0.99	219.8
15-c36	1.04	204.4
15-c900	1.04	195.4
15-vac	1.03	204.3
45	0.80	251.9
45-c12	0.99	202.8
45-c36	1.05	212.8
45-c900	1.06	191.9
45-vac	0.98	191.2

4.1.4. Electrical Conductivity

One of the most important parameters that determine EDLC performance of activated carbons is electrical conductivity. The structure and surface functional groups of activated carbons have a great influence on electrical conductivity, as Table 5 demonstrates. In the model suggested by Mrozowski [65], electronic energy band of carbons are given as a function of heat treatment temperature. The reduction of band gap, and consequently increase in conductivity is associated with delocalized electrons of π bonds, which reside in sp^2 clusters of aromatic rings. The Raman spectra of the activated carbons indicate that sp^2 cluster size increases after high temperature heat treatment with aromatic ring condensation. Furthermore, surface oxygen groups decrease electronic conductivity of activated carbons, since they occupy the edges of the microcrystalline domains and blocking the electron transfer [66]. FTIR spectra of the produced activated carbons provide evidence to decrease surface oxygen groups upon vacuum and CO_2 heat treatment.

As a result, electronic conductivities of vacuum and CO_2 treated samples increase 5 orders of magnitude, for higher sp^2 cluster size and lower surface oxygen content.

Table 5. Electrical conductivities of activated carbons.

	Conductivity (S/cm)
15	$2.1x10^{-5}$
45	$2.6x10^{-5}$
15-c12	0.60
45-c12	0.34
15-c36	0.37
45-c36	0.32
15-c900	0.74
45-c900	0.60
15-vac	0.98
45-vac	0.72

4.1.5. Scanning Electron Microscopy

SEM micrographs of pine cones and activated carbons are given in Figure 22. Residuals of crushed lignocellulosic structure and macropores already present in this structure are evident in a and b. All of the produced activated carbons have irregular shapes based on this structure. 4 impregnation ratio samples have rougher surfaces compared to 1 impregnation ratio ones. Furthermore, the difference between CO_2 and vacuum treatment on macroporosity can be seen in the micrographs. Since there is no activating agent in vacuum treatment, the morphologies of the particles do not greatly change as a result of it. However, carbons continue to develop porosity in CO_2 treatment; and this causes erosion of the surface, which brings about development of macroporosity [20]. Comparing e, f, and g, it can be concluded that this effect is more pronounced for 1 impregnation ratio samples and for high burn off degree CO_2 treated ones. The size of

macropores created by CO_2 treatment is in the order of several micrometers; therefore, they have a limited influence on the adsorption behavior and they are disregarded in the surface area calculations. However, this large pores reduces the density of the material, hence it is estimated that EDLC's constructed with them have low volumetric energies.

Table 6 shows the chemical compositions of pine cone and activated carbons. Pine cone has considerable amount of oxygen and small amount of potassium and chlorine as it is an organic matter containing minerals. Other elements were not detected in EDS analyses due to low ash content of the pine cones. However, EDS analysis on ash of pine cone shows additionally sodium (2 wt. %), magnesium (7 wt. %), phosphorus (14 wt. %) and sulfur (3 wt. %). As a result of carbonization, oxygen amount is greatly reduced. Chemical activation with $ZnCl_2$ brings about complete disappearance of potassium and possibly the other elements shown in the ash analysis [25]. However, chlorine content is high in samples 15 and 45 due to chlorine comes from $ZnCl_2$. After vacuum and CO_2 treatments, both oxygen and chlorine content further decrease since surface functional groups are released.

Table 6. EDS analysis of pine cone and activated carbons.

	C (wt. %)	O (wt. %)	Cl (wt. %)	K (wt. %)
Pine cone	64.1	35.5	0.1	0.3
15	94.1	4.9	1.0	-
45	93.6	5.4	1.0	-
15-vac	97.0	2.7	0.3	-
45-vac	96.3	3.4	0.3	-
15-c12	96.7	2.9	0.4	-
45-c12	96.0	3.8	0.2	-
15-c36	97.7	2.0	0.3	-
45-c36	97.8	2.1	0.1	-
15-c900	98.4	1.3	0.3	-
45-c900	98.5	1.2	0.3	-

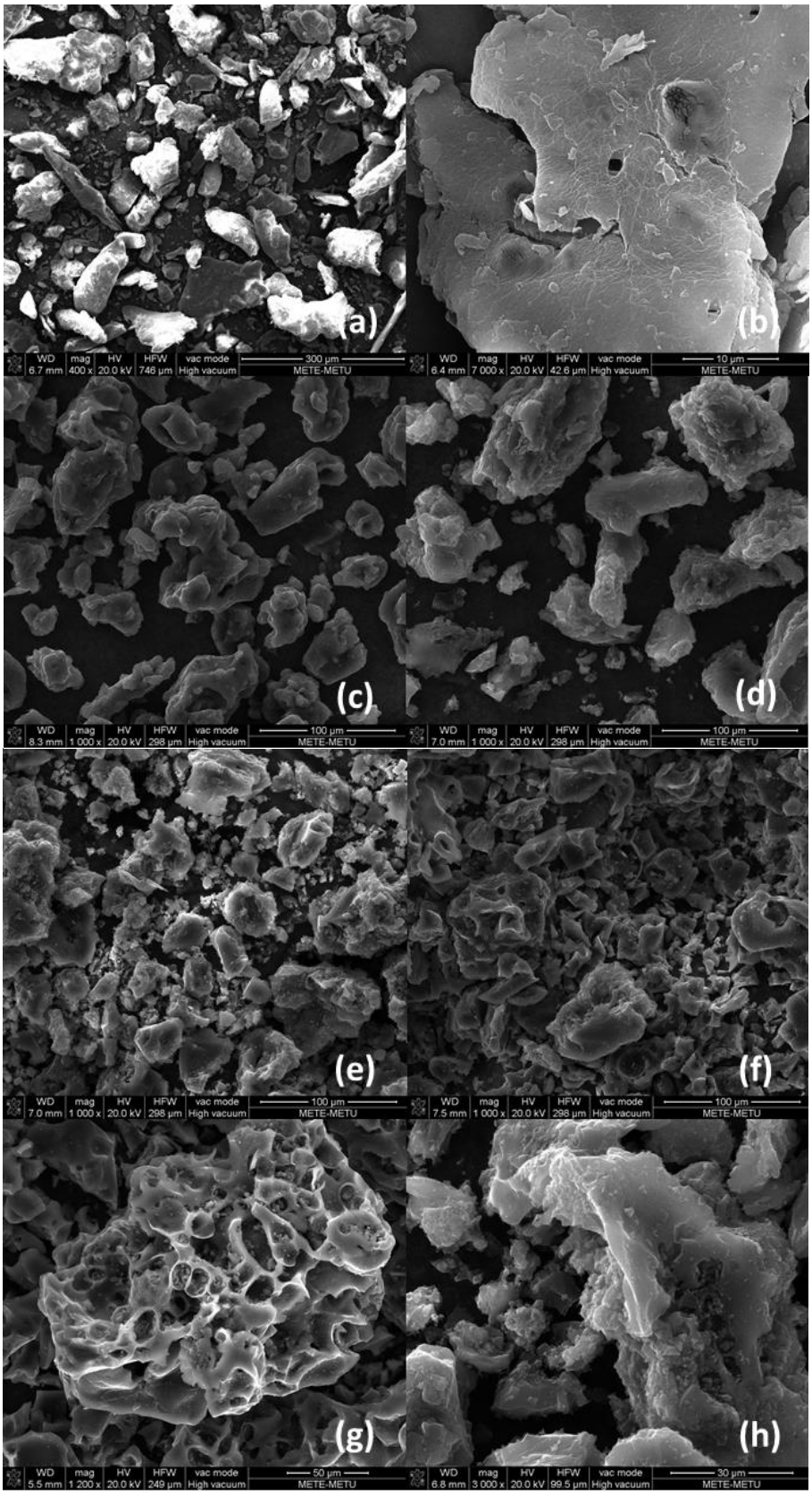
(a)
WD 6.7 mm | mag 400 x | HV 20.0 kV | HFW 746 µm | vac mode High vacuum | 300 µm | METE-METU
(b)
WD 6.4 mm | mag 7 000 x | HV 20.0 kV | HFW 42.6 µm | vac mode High vacuum | 10 µm | METE-METU
(c)
WD 8.3 mm | mag 1 000 x | HV 20.0 kV | HFW 298 µm | vac mode High vacuum | 100 µm | METE-METU
(d)
WD 7.0 mm | mag 1 000 x | HV 20.0 kV | HFW 298 µm | vac mode High vacuum | 100 µm | METE-METU
(e)
WD 7.0 mm | mag 1 000 x | HV 20.0 kV | HFW 298 µm | vac mode High vacuum | 100 µm | METE-METU
(f)
WD 7.5 mm | mag 1 000 x | HV 20.0 kV | HFW 298 µm | vac mode High vacuum | 100 µm | METE-METU
(g)
WD 5.5 mm | mag 1 200 x | HV 20.0 kV | HFW 249 µm | vac mode High vacuum | 50 µm | METE-METU
(h)
WD 6.8 mm | mag 3 000 x | HV 20.0 kV | HFW 99.5 µm | vac mode High vacuum | 30 µm | METE-METU

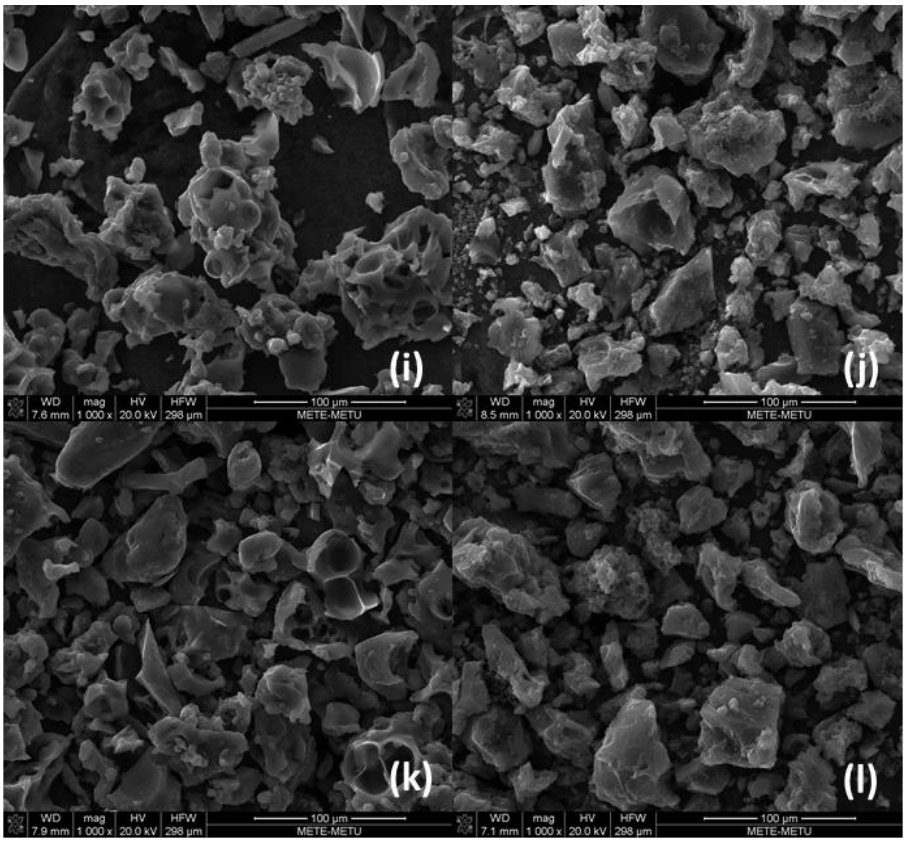

Figure 22. SEM micrographs of pine cone (a, b) and samples 15 (c), 45 (d), 15-vac (e), 45-vac (f), 15-c12 (g), 45-c12 (h), 15-c36 (i), 45-c36 (j), 15-c900 (k), 45-c900 (l).

4.2. Electrochemical Characterization

Electrical double layer capacitor studies on produced activated carbons are given in three sections. In the evaluation of EDLC performance, binder used in the electrode preparation, conductivity of the activated carbons and porous structure change upon heat treatment applied are the most influential parameters. Therefore, their effects on the EDLC behavior of these three parameters are given separately. In the first section, the effect of two binders (PSBR 100 and LA 132) is discussed, with their application to one of the vacuum treated carbons. The second section is

based on the performance of vacuum treated carbons, and evaluation of CO_2 treated carbons is given in the final section.

4.2.1. Effect of Binder in EDLC Performance

Cyclic voltammetry of EDLC's constructed with vacuum treated 45-vac sample and LA 132 and PSBR 100 is given in Figure 23. Two electrolytes are used: TEA BF_4 and TBA PF_6 dissolved in acetonitrile. They all have quasi-rectangular voltammograms, which shows the capacitive charge storage upon applied voltage. However, samples prepared with LA 132 binder (Figure 23, a) has a deformed shape; i. e. the edges of the rectangles are more rounded than the ones that EDLC's with PSBR 100 binder. The reason of this shape difference is the resistance of the cells; the more resistive behavior, the more rounded the shape of the voltammograms. Furthermore, electrochemical impedance spectroscopy results remark an order of magnitude larger diameter of high frequency loop in cells with LA 132 binder as seen in Figure 24, which is a measure of cell resistance in EDLC's. Therefore, it is deduced from both qualitative evaluations of the voltammograms and EIS data, that LA 132 binder has a more resistive character, consistent with the previous study based on LA 135 binder [13].

The electrolyte effect is also seen in the cyclic voltammograms. The performance of TEA BF_4 salt is superior in both cells with LA 132 and PSBR 100 binder. There is a current decrease in cells with TBA PF_6 electrolytes at high voltages, especially pronounced in the LA 132 binder. This effect is associated with porosity saturation, which will be detailed in later sections. Furthermore, the current densities reached by EDLC's with TBA PF_6 electrolyte behave differently in two binders. The current density in TBA PF_6 with LA 132 binder achieves nearly the same value as TEA BF_4 in the same binder for voltages up to 0.7 volts; however, current density is always smaller in cells with TBA PF_6 electrolyte than TEA BF_4 electrolyte with PSBR 100 binder. The reason of this situation can be the

difference in the ion diffusion in the binders. TBA^+ ion diffusion is more restricted in the PSBR 100 binder so that cell with TBA PF_6 cannot reach the same value as it reaches in the LA 132 binder.

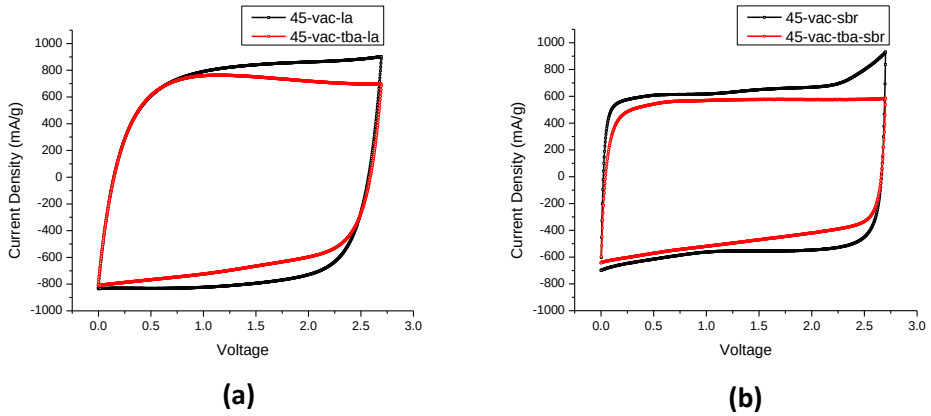

Figure 23. Cyclic voltammograms of vacuum treated carbons produced by using a) LA 132 and b)PSBR 100 binder at 30 mV/s.

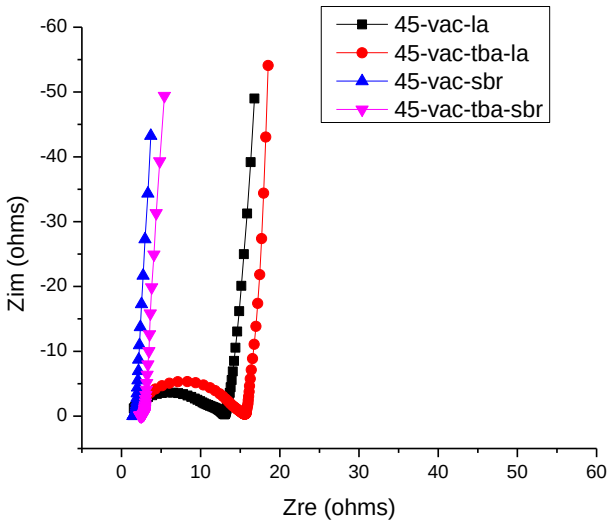

Figure 24. Nyquist plots of the EDLC's.

The ion diffusion problem is more evident in evaluating specific capacitances as seen in Table 7. The EDLC's with PSBR 100 binder have substantially smaller specific capacitances. Since ion diffusion is more restricted in PSBR 100 binder, ions cannot reach the pores where they form double layer, deteriorating specific capacitance values.

Considering EDLC's can be optimized for either high power density or high energy density, these two binders are both used for their superior performances on either resistance or capacitance. Moreover, pore size effect on power and energy density is also considered; narrow pore size carbons are superior in the capacitive performance, but worse in power. Regarding these parameters, while LA 132 binder, more capacitive and also resistive, is used in the production of vacuum treated activated carbons having smaller average pore size, PSBR 100 binder is used for larger pore size CO_2 treated carbons to achieve high power density.

Table 7. Specific capacitances of the EDLC's at 10 mV scan rate.

	Sp. Cap. (F/g)
45-vac-la	92.8
45-vac-tba-la	82.0
45-vac-sbr	79.9
45-vac-tba-sbr	67.9

4.2.2. Capacitive Properties of Non-heat treated Activated Carbons

Cyclic voltammograms of non-heat treated activated carbons (samples 15 and 45) with TEA BF_4 in acetonitrile electrolyte are given in the Figure 25. The figure demonstrates that these carbons do not reflect the typical quasi-rectangular voltammograms of carbon materials; rather they show resistive behavior. In a previous study [67], similar treatments with $ZnCl_2$ resulted in similar cyclic voltammetry responses. They concluded this response results from porous

structure of the carbons produced. Although this may have an effect on the resistive behavior, as sample 45 with a pronounced mesoporosity suggests a better reaction especially in higher applied voltages, the 5-fold increase in the electrical resistivity when compared with vacuum treated carbons clarifies that the main contribution to overall capacitor resistance comes from the resistivity of the activated carbons. Furthermore, higher amount of oxygen functional groups in 45 can have a pseudocapacitive effect on electrochemical behavior, which can be the reason for high current density in high potential difference. Comparing cyclic voltammetry response of sample 45 at 10 mV/s and 50 mV/s, a decrease in the current density is observed in sample 45. This is the result of limited diffusion at high scan rates, even further deteriorating the capacitance.

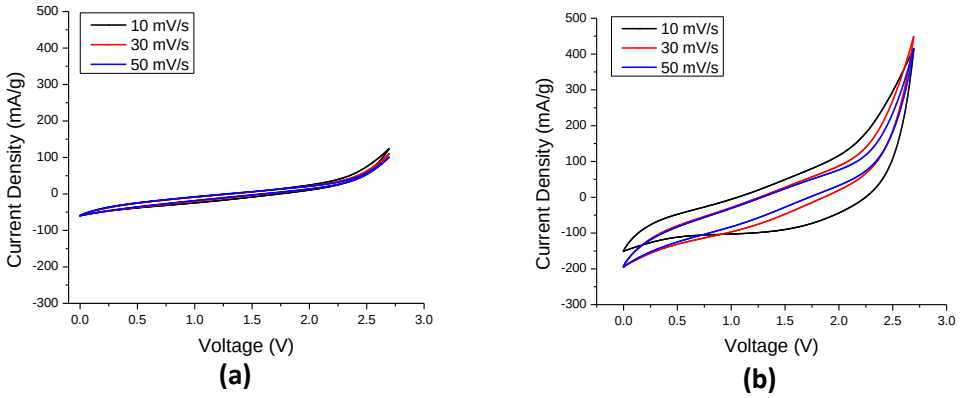

Figure 25. Cyclic voltammograms of untreated a) 15 and b) 45 samples at scan rates of 10, 30 and 50 mV/s.

4.2.3. CO_2 Treated Activated Carbons for High Power EDLC's

Figures 26, 27 and 28 show the cyclic voltammetry and galvanostatic charge and discharge curves of CO_2 treated activated carbons prepared with PSBR 100 binder, with two electrolytes (TEA BF_4 and TBA PF_6) at various scan rates and currents.

Comparing cyclic voltammograms of non-heat treated activated carbons (15 and 45) with the CO_2 treated ones; the effect of heat treatment on the EDLC performance of activated carbons is evident. The latter ones have rectangular voltammograms, reaching about 1 A/g current densities at 50 mV/s scan rates. The reason of this observation is attributed mainly to 5 orders of magnitude electrical conductivity enhancement with high temperature heat treatment. Effect of porosity on resistive behavior of non-heat treated activated carbons is proven to be negligible compared to electrical conductivity; as the most open structure with the largest surface area and pore size is in sample 45.

The effect of scan rate increase on cyclic voltammetry and current increase on galvanostatic charge and discharge is similar; scanning at a higher rate increases the current in cyclic voltammetry, and charging and discharging at a higher current decreases charge-discharge time. This is clearly seen in Figures 26, 27 and 28.

Galvanostatic charge and discharge curves in Figures 26, 27 and 28 show typical EDLC characteristics. There is a linear increase in potential upon charging at constant current, and a linear decrease in potential upon discharging. The curves are nearly symmetrical, although discharge curves are slightly more sloping. There is a decrease in potential at the beginning of discharge, called IR drop. This reduction at the beginning of discharge is linked to resistance of the cell and equivalent series resistances are calculated according to them. As the current increases, so does IR drop, which limits the performance of EDLC's at high currents.

Moreover, current densities reached by EDLC's in cyclic voltammetry using TEA BF_4 electrolyte are superior to EDLC's with TBA PF_6 at all scan rates for all samples. This is also evidenced with galvanostatic charge-discharge curves, in which charge discharge times of EDLC's with TEA BF_4 electrolyte are all longer. This behavior is associated with restricted TBA^+ ion diffusion in PSBR 100 binder as indicated in the previous sections, preventing the double layer formation

especially at low potentials. Thus, specific capacitance reached with TEA BF_4 salt is higher, due to limited ionic diffusion for TBA^+.

What is more, current densities of carbons with different pore characteristics are similar in TEA BF_4 electrolyte, while capacitive current drops as the voltage is increased in TBA PF_6. Pore saturation, complete coverage of the available surface before reaching the maximum voltage as a result of insufficient development of porosity, is the reason of the capacitance reduction at high voltages. Comparing CV results of 4 impregnation ratio and 1 impregnation ratio samples with TBA PF_6 electrolytes, high effective surface area values of the former ones for TBA^+ electroadsorption prevents saturation of porosity, while the latter ones exhibit this current decrease, being more pronounced for 15-c12. This is more clearly seen as the scan rate is increased in cyclic voltammetry and current is increased in galvanostatic charge and discharge. Comparison of Figures 26 (e, f), 27 (e, f) and 28 (e, f) illustrates the impact of pore size; as the surface area and average pore volume of the activated carbon increases, porosity saturation effect disappears.

Specific capacitances are drawn as a function of DFT specific surface areas of activated carbons in Figure 29. There is no trend found in the specific capacitance values as specific surface area changes, consistent with previous studies [39, 40]. The lack of capacitance enhancement with increasing surface area was attributed to the charge screening in the article published by Barbieri *et. al*. [40]; development of surface area diminishes pore wall thickness, thus, electric potential within the pore does not reach zero, which deteriorates capacitive behavior so that specific capacitance remains constant for carbons having specific surface areas larger than 1200 m^2/g, no matter how specific surface area enhances.

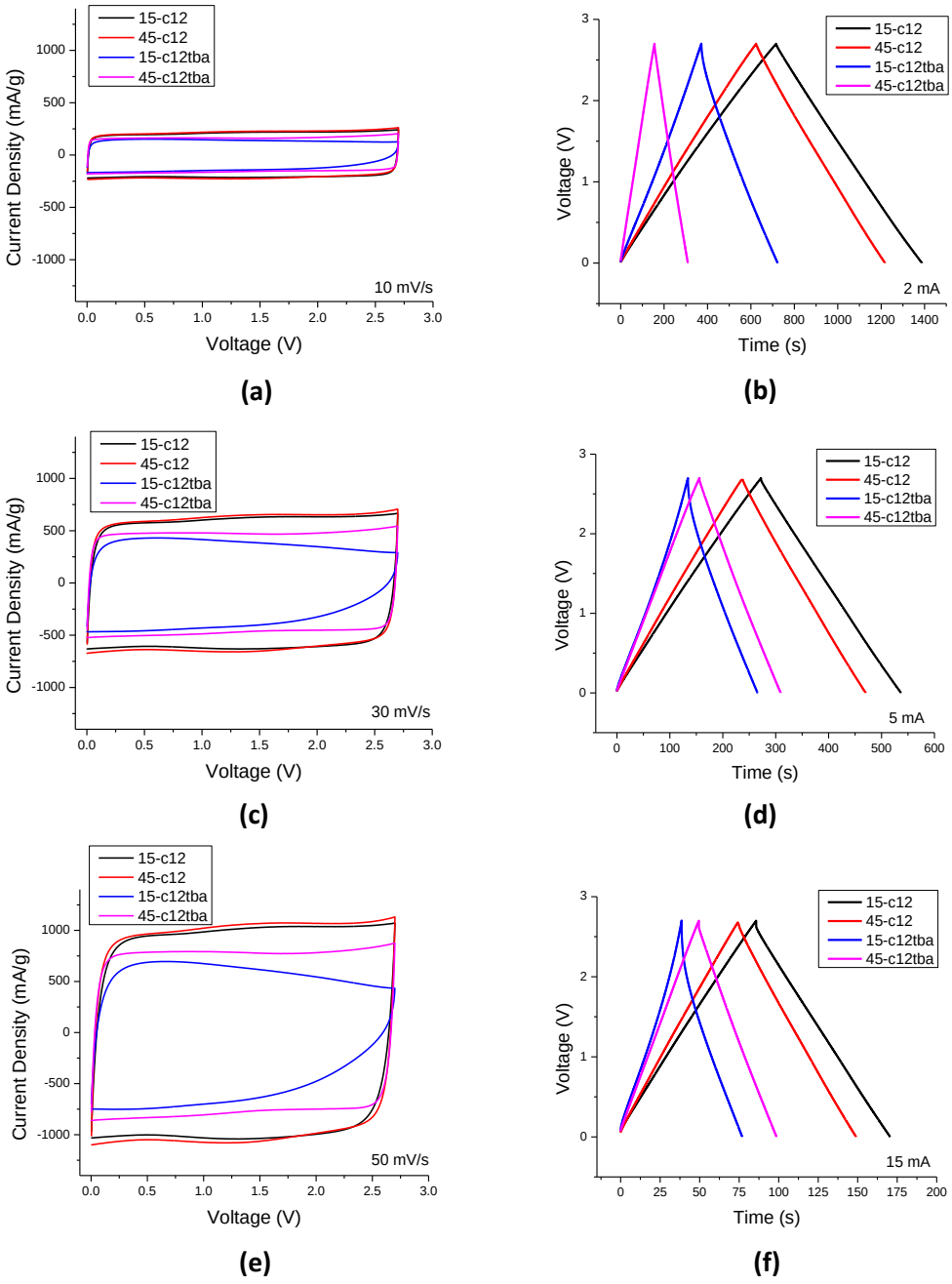

Figure 26. Cyclic voltammograms and galvanostatic charge discharge curves of CO_2 treated carbons at 800 °C for 12 hours with TEA BF_4 and TBA PF_6 electrolyte. Cyclic voltammetries are scanned at a rate of a) 10 mV/s, c) 30 mV/s, e) 50 mV/s, and charge-discharge curves are obtained at a current of b) 2 mA, d) 5 mA, and f) 15 mA.

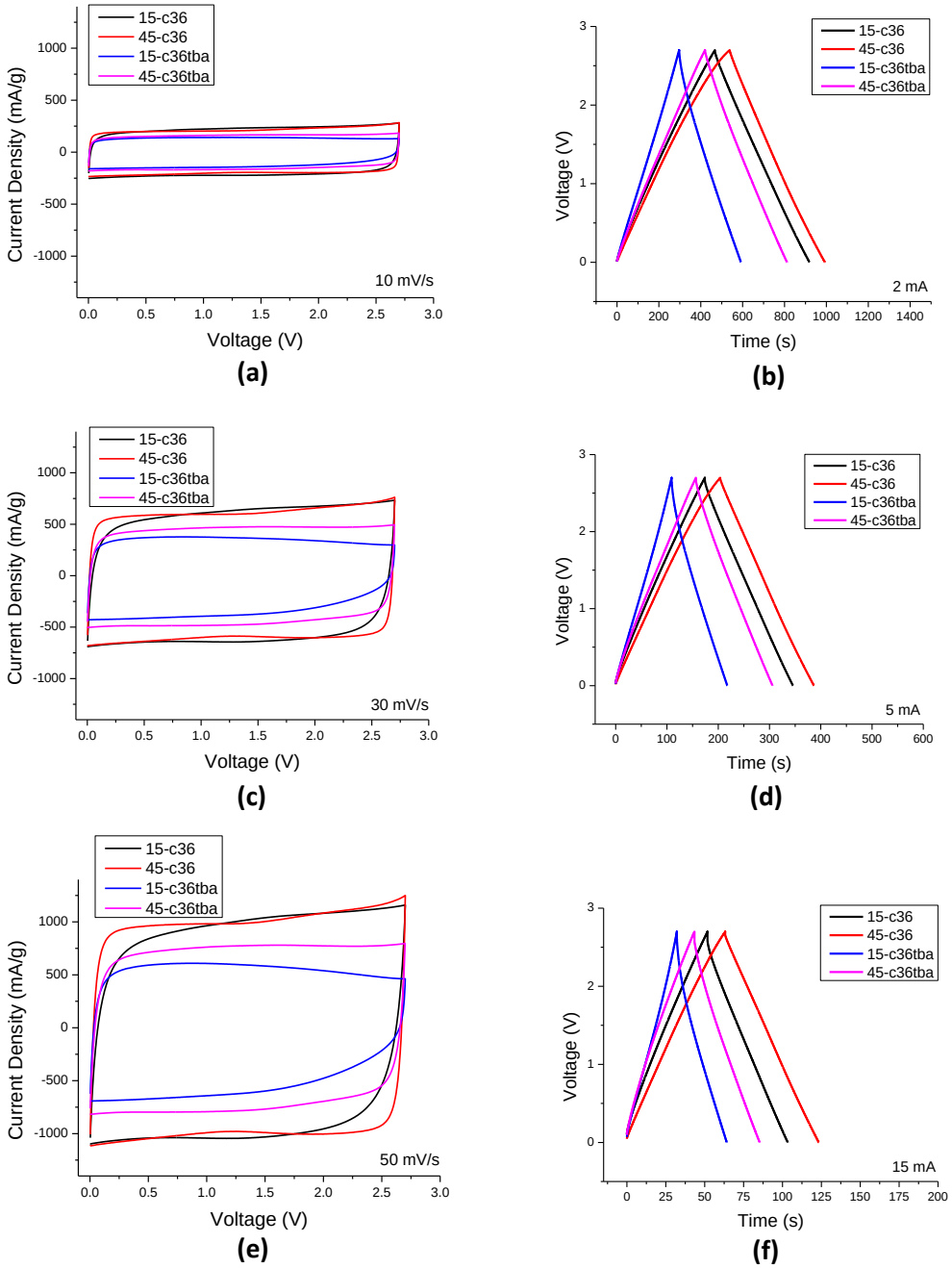

Figure 27. Cyclic voltammograms and galvanostatic charge discharge curves of CO_2 treated carbons at 800 °C for 36 hours with TEA BF_4 and TBA PF_6 electrolyte. Cyclic voltammetries are scanned at a rate of a) 10 mV/s, c) 30 mV/s, e) 50 mV/s, and charge-discharge curves are obtained at a current of b) 2 mA, d) 5 mA, and f) 15 mA.

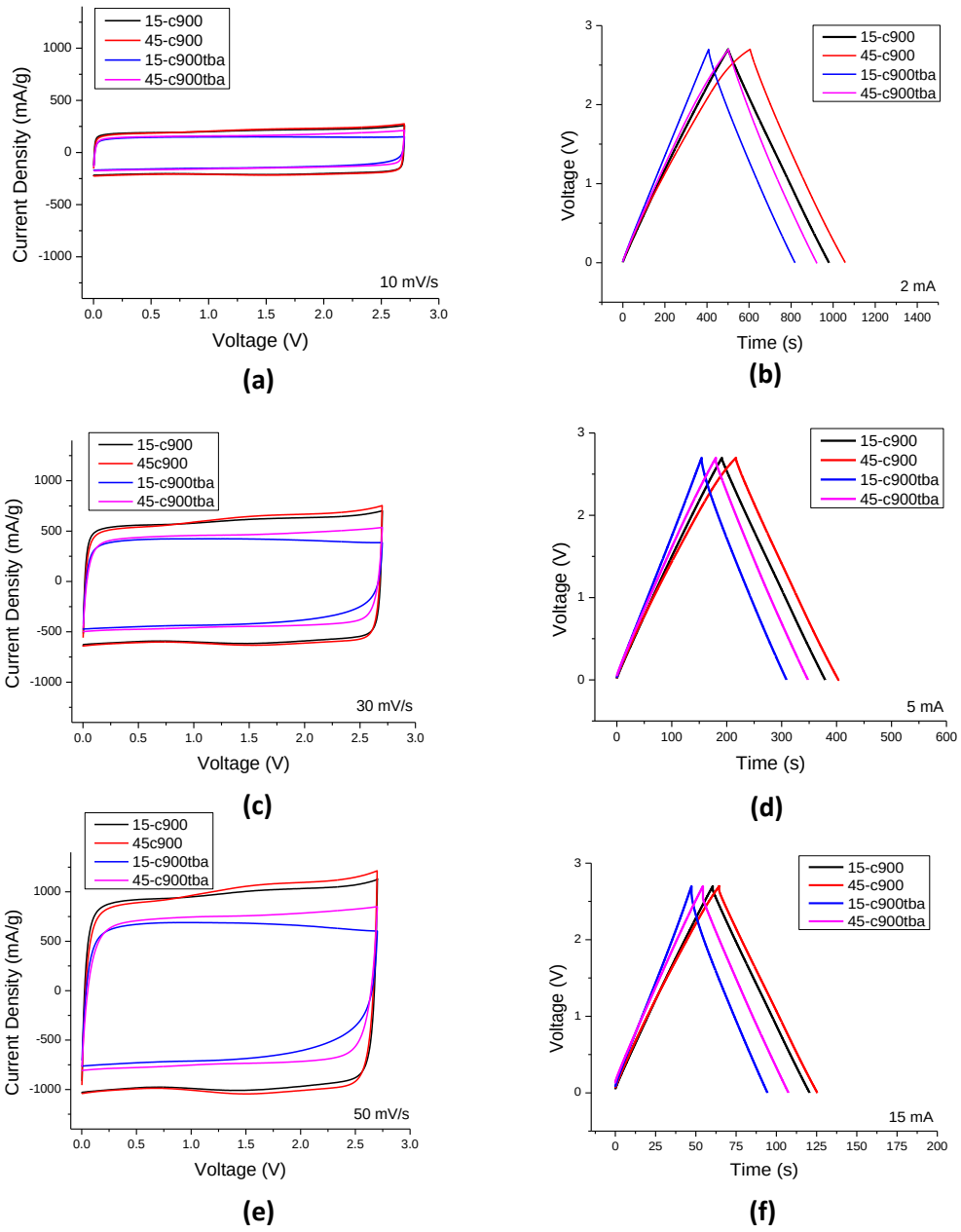

Figure 28. Cyclic voltammograms and galvanostatic charge discharge curves of CO_2 treated carbons at 900 °C for 5 hours with TEA BF_4 and TBA PF_6 electrolyte. Cyclic voltammetries are scanned at a rate of a) 10 mV/s, c) 30 mV/s, e) 50 mV/s, and charge-discharge curves are obtained at a current of b) 2 mA, d) 5 mA, and f) 15 mA.

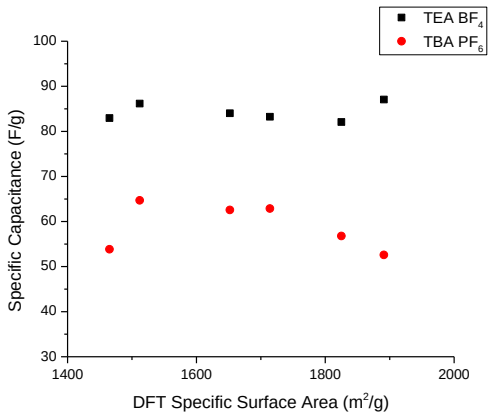

Figure 29. Specific capacitance vs. Specific surface area of the activated carbons.

The impact of pore structure on the double layer performance of carbons has been a subject of controversy. In an earlier approach, ions are accepted as in their solvated state at the double layer. Therefore, carbons having pore widths greater than 1 nm is argued to be superior in EDLC's. More recently, microporous carbons with smaller average pore sizes and narrower pore size distributions are suggested to have higher specific capacitance per unit area [38]. This behavior originates from desolvation of ions in their charged state [40]. Therefore, bare ion sizes (TEA^+:0.68 nm, TBA^+:0.82 nm) are used in this study to evaluate electrochemical behavior [42]. The effect of anion size is not taken into account due to their relatively small size.

The capacitive properties of the carbons are further analyzed with normalizing specific capacitance values by available surface areas in Table 8. Similar trends are observed for both electrolytes: a dramatic reduction of capacitance with enhancement of the average pore size, L_0. Ineffective usage of pore volume in wide pores brings about this reduction in normalized capacitance. Furthermore, although the trend is similar, EDLC's with TEA BF_4 electrolyte have high normalized capacitance for all samples. This is linked to the bigger size of the TBA^+ cation, increasing the distance between electrode surface and ions. Although

similar specific capacitances are obtained with the activated carbons of different porosities, the use of narrow pore size activated carbons in EDLC applications is beneficial, regarding effective surface area utilization.

Specific capacitance change as a function of scan rate is given in Table 9. Specific capacitance reduction with increasing scan rate is observed for all samples. The reason of this reduction is the limitation of the ion diffusion at high rates of charge and discharge. Due to limited diffusion, some of the ions do not have enough time to reach electrode surface and form double layer, so that capacitance decreases. However, a relatively stable behavior arises in the EDLC's with TEA BF_4 electrolyte. Diffusion is more restricted for TBA^+ ions in the TBA PF_6 electrolyte due to its bigger size and low concentration, therefore its capacitance reduction is more pronounced with increasing scan rates. Furthermore, porous structure affects capacitive response as a function of scan rate; greater capacitance reduction of narrow pore size 1 impregnation ratio samples in TBA PF_6 electrolyte results from their porous characteristics.

Table 8. Average pore sizes, available surface areas and normalized capacitances of CO_2 treated activated carbons.

	L_0 (nm)	S_{DFT}>0.68 (m^2/g)	S_{DFT}>0.82 (m^2/g)	C_{TEA}^+/S_{DFT}>0.68 ($\mu F/cm^2$)	C_{TBA}^+/S_{DFT}>0.82 (µF/cm2)
15c12	0.89	725	516	11.4	10.4
15c36	0.93	1022	744	8.5	7.1
15c900	0.96	1079	770	7.6	7.3
45c12	1.49	1154	1026	7.4	6.3
45c36	1.55	1377	1201	6.0	5.2
45c900	1.55	1313	1156	6.3	5.4

Table 9. Specific capacitances evaluated in cyclic voltammetry as a function of scan rate for CO_2 treated samples.

C_{CV} (F/g)	10 mV/s	30 mV/s	50 mV/s
15-c12	82.9	79.2	76.8
15-c36	87.1	79.8	75.5
15-c900	82.1	78.6	76.8
45-c12	86.2	82.1	79.8
45-c36	83.3	80.8	79.5
45-c900	84	80.4	78.6
15-c12tba	53.8	48.6	45.7
15-c36tba	52.6	45.6	43.3
15-c900tba	56.8	52.9	50.9
45-c12tba	64.7	62.6	61.4
45-c36tba	62.9	59.6	57.9
45-c900tba	62.6	59.3	57.4

4.2.4. Vacuum Treated Activated Carbons for High Energy EDLC's

Vacuum treated activated carbons are prepared with LA 132 binder and two electrolytes (TEA BF_4 and TBA PF_6), and their cyclic voltammetry and galvanostatic charge-discharge curves are given in Figure 30. Qualitative analysis of these curves remarks that the capacitive response in both cyclic voltammetry and galvanostatic charge and discharge are similar to that of EDLC's prepared with CO_2 treated carbons; a dramatic increase in current density resulting from scan rate increase in cyclic voltammetry, and low charge-discharge times as current increases in galvanostatic charge and discharge. However, their rectangular shapes of voltammograms scanned at 10 mV/s are deteriorated in the scan at 50 mV/s. Also, their IR drop values reach about 0.5 Volts at 15 mA current density. Both of these situations indicate that the power performance of the EDLC's are getting worse as the rate of charge and discharge increases, inferior to EDLC's with CO_2 treated activated carbons in PSBR 100 binder.

Capacitive performance limitation by porosity saturation appears to be pronounced in 15-vactba; in fact, current density drops nearly zero at voltages close to 2.7 V. This effect is also clear in the charge-discharge curve. Dramatic drop in voltage at the beginning of discharge in Figure 30 (d, blue curve) is not associated with resistance of the cell; it has also contributions from narrowing effect of porosity saturation on the voltage profile. Current drop can be seen in the voltammogram of 45-vactba; however, it is not as high as the one in 15-vactba.

As discussed in the previous sections diffusion is less restricted in the cells with LA 132 binder. This has an impact on both specific capacitance and current densities reached by EDLC's with TEA BF_4 and TBA PF_6 electrolytes at low scan rates. Specific capacitance calculated at low scan rates from cyclic voltammetry and low currents from discharge curves are greater for the cells with LA 132 binder. In fact, a specific capacitance value of 113 F/g is reached with 45-vac sample with TEA BF_4 electrolyte, one of the best results reported in literature for $ZnCl_2$ activated carbons with organic electrolytes.

The effect of pore ion interactions on capacitive properties can be analyzed clearly as diffusion is less limited and all of the porosity is assumed to be open for double layer formation. Average pore sizes, effective surface areas and normalized capacitances (by effective surface area) are given in Table 10. First of all, effect of average pore size has a dramatic effect on normalized capacitance, which reduces with pore size enhancement. The reduction is also observed for CO_2 treated carbons; however, it is sharper for vacuum treated ones. Furthermore, capacitances normalized by effective surface area in both carbons are nearly the same for the EDLC's with both electrolytes. Considering current density is nearly equal for both electrolytes with TEA^+ and TBA^+ cations at low potentials, and distortion of cations in the pores smaller than their desolvated sizes when the electrodes are polarized [43], this can be explained by more severely deformation of TBA^+ cation when electroadsorbed into narrow micropores. As a consequence, effective surface area calculation based on rigid cation size is not strictly true. Hence, assuming

larger effective surface area values especially for TBA^+ cation seems to be reasonable. However, normalized capacitance values are found to be nearly the same for both electrolytes in the same activated carbon, while EDLC's with TBA PF_6 electrolyte are expected to have bigger values based on the above argument. Since bigger size TBA^+ cations occupy more surface area in the pores, and also utilize pore volume ineffectively into the larger pores, effective surface area enhancement due to distortion does not result in normalized capacitance increase.

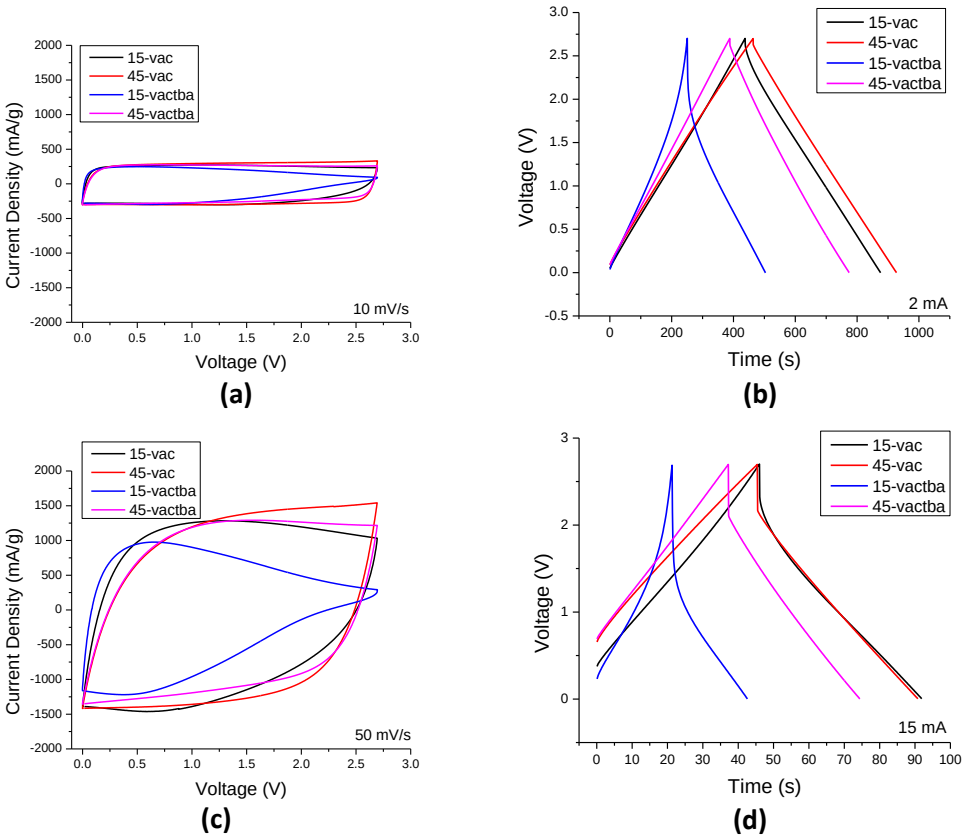

Figure 30. Cyclic voltammograms and galvanostatic charge discharge curves of vacuum treated carbons with TEA BF_4 and TBA PF_6 electrolyte. Cyclic voltammetries are scanned at a rate of a) 10 mV/s, c) 50 mV/s, and charge-discharge curves are obtained at a current of b) 2 mA, d) 15 mA.

Table 10. Average pore sizes, available surface areas and normalized capacitances of vacuum treated activated carbons.

	L_0 (nm)	S_{DFT}>0.68 (m^2/g)	S_{DFT}>0.82 (m^2/g)	C_{TEA}^+/S_{DFT}>0.68 (µF/cm^2)	C_{TBA}^+/S_{DFT}>0.82 (µF/cm2)
15-vac	0.81	554	375	17.7	17.5
45-vac	1.33	1072	913	10.4	10.8

Table 11 demonstrates specific capacitance reduction related to rate increase in both cyclic voltammetry and galvanostatic charge and discharge. Comparing this reduction with the EDLC's with CO_2 treated samples in PSBR 100 binder, rate performance of these cells are inferior. Specific capacitance decreases nearly 80% of its low rate value at high scan rates and current densities. The main reason of this capacitance loss cannot be attributed to porosity shrinkage in vacuum treated activated carbons; relatively wide pore size 45-vac sample has the same reduction in both electrolytes. Therefore, this behavior is linked to electrode preparation step, especially to binder. As a result, this cell construction brings about high specific capacitances at low currents due to less restricted ion diffusion; however, capacitance loss at high currents can be a limitation in its usage and further studies focusing on optimization of its properties are needed.

Table 11. Specific capacitances evaluated in cyclic voltammetry as a function of scan rate for vacuum treated samples.

C (F/g)	10 mV/s	30 mV/s	50mV/s
15-vac	98.5	88.3	80.3
45-vac	111.6	96.9	83.7
15-vactba	66.4	55.3	49.7
45-vactba	98.7	86.2	76.3

4.2.5. Overall Performance Evaluation of EDLC's

The performance of the EDLC's are evaluated by Ragone plot given in Figure 31. Energy density range is nearly 10-30 Wh/kg, and power density range is about 100-2000 W/kg. Both power and energy densities of EDLC's with TEA BF_4 electrolyte are superior to that of EDLC's with TBA PF_6 electrolyte, due to limited diffusion of TBA^+ ions and ineffective surface area usage. Furthermore, energy densities reached by vacuum treated carbons with LA 132 binder is higher than others; 28 Wh/kg energy density is reached by sample 45-vac with TEA BF_4 electrolyte. However, increasing power density has a detrimental effect on the energy density of these EDLC's. On the other hand, EDLC's with CO_2 treated carbons have relatively stable energy density as power density is raised, which makes them candidates for high power applications.

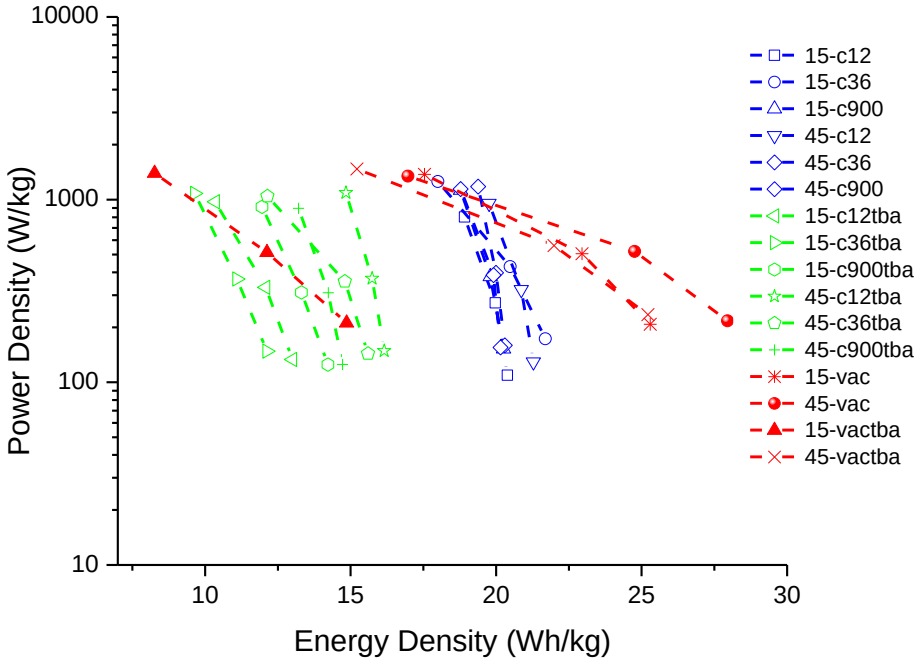

Figure 31. Ragone plot for EDLC's.

Equivalent series resistances and maximum power densities achievable by the EDLC's are given in Table 12. There is no correlation found between average pore size of the activated carbons and equivalent series resistances. Rather, electrolyte and binder used in the electrode preparation affects ESR and maximum power density dramatically. ESR values of vacuum treated carbons with LA 132 binder is an order of magnitude higher than that of CO_2 treated carbons with PSBR 100 binder. Sample 45-c36 has the lowest ESR (1.45 Ω) and the highest maximum power density (71.8 kW/kg), achieving one of the highest maximum power density of $ZnCl_2$ activated carbons in organic electrolytes.

Table 12. Equivalent series resistance (ESR) and maximum power density P_{max} of the EDLC's.

	ESR (Ω)	P_{max} (kW/kg)
15-c12	1.92	38.4
15-c36	3.52	33.0
15-c900	1.48	67.2
45-c12	1.67	52.2
45-c36	1.45	71.8
45-c900	1.89	53.4
15-c12tba	2.68	33.1
15-c36tba	2.67	36.9
15-c900tba	2.50	33.6
45-c12tba	2.40	41.1
45-c36tba	3.01	31.6
45-c900tba	4.19	20.0
15-vac	13.80	9.4
45-vac	17.79	8.0
15-vactba	17.85	5.6
45-vactba	19.4	7.9

CHAPTER 5

CONCLUSIONS

Activated carbons with various structural and textural characteristics were produced for EDLC applications. The production routes of activated carbons included two steps: chemical activation with $ZnCl_2$ at 500 °C, and vacuum or CO_2 treatments at 800, 900 and 950 °C for various periods. Both microporous and micro + mesoporous activated carbons were produced with 1 and 4 impregnation ratios after $ZnCl_2$ activation. Vacuum treatment did not result in further evolution of surface area and pore volume as there was no activating agent present, instead, porosity shrinkage occured. On the other hand, CO_2 acted as a physical activating agent and further evolved porosity. Burn off degree was found to be the most important parameter for the resulting porous structure. As a consequence, activated carbons with DFT surface areas ranging from 1300 to 2700 m^2/g were produced with various pore size distributions.

Post treatments applied to $ZnCl_2$ activated samples had a pronounced effect on both surface functional groups and structural order. Only $ZnCl_2$ activated carbons possessed large number of surface functional groups, whereas they were significantly reduced for both vacuum and CO_2 treated carbons, identified by FTIR analysis. Furthermore, their structural evolution were strongly dependent on treatment temperature; intensity ratios of D and G bands, and FWHM of the D band in Raman spectra remarked that vacuum and CO_2 treated samples at elevated temperatures were more ordered than only $ZnCl_2$ activated carbons. The fact that samples only activated with $ZnCl_2$ had more surface functional groups and lack ordering dramatically impacted electrochemical behavior. As a result of their resistive nature, they did not show ideal capacitive behavior. Successful electrochemical results were obtained from vacuum and CO_2 treated samples.

Electrochemical behaviors of the EDLC's were affected from characteristics of the activated carbons (porous structure, surface functional groups and structural order), electrolyte (TEA BF_4 and TBA PF_6) and binder (LA 132 and PSBR 100). LA 132 binder was found to be superior in capacitive performance and suitable for high energy density EDLC's, while PSBR 100 binder was suitable for high power devices. Considering the capacitance improvement when pore size of the active material match with size of the ions in desolvated states, narrow pore size vacuum treated samples were used with LA 132 binder to obtain high energy density EDLC's. As a consequence, 113 F/g and 98 F/g specific capacitances were achieved in TEA BF_4 electrolyte for samples 45-vac and 15-vac, respectively. The capacitances of EDLC's with smaller size cation electrolyte (TEA BF_4) were superior for all samples as a result of diffusion limitation and inefficient surface area usage in large size cation TBA PF_6. Although specific capacitance did not clearly depend on pore size and surface area, capacitance normalization by available surface area displayed that microporous carbons with smaller average pore size were more effective in capacitive storage of ions.

REFERENCES

1. Winter, M., & Brodd, R. J. (2004). What are batteries, fuel cells, and supercapacitors? *Chemical Reviews*, *104*(10), 4245-4270.

2. Halpin, S. M., Nelms, R. M., & Schatz, J. E. (1997, November). Characterization of double-layer capacitor application issues for commercial and military applications. In *Industrial Electronics, Control and Instrumentation, 1997. IECON 97. 23rd International Conference on* (Vol. 3, pp. 1074-1079). IEEE.

3. Yu, A., Chabot, V., & Zhang, J. (2013). *Electrochemical supercapacitors for energy storage and delivery: fundamentals and applications* (pp. 37-95). Boca Raton, FL: CRC Press.

4. Becker, H. I. (1957). *U.S. Patent No. 2,800,616*. Washington, DC: U.S. Patent and Trademark Office**.**

5. Conway, B. E. (2013). *Electrochemical supercapacitors: scientific fundamentals and technological applications* (pp. 11-31). New York, NY: Kluwer Academic/ Plenum Publishers.

6. Kötz, R., & Carlen, M. (2000). Principles and applications of electrochemical capacitors. *Electrochimica Acta*, *45*(15), 2483-2498.

7. Bard, A. J., Faulkner, L. R., Leddy, J., & Zoski, C. G. (1980). *Electrochemical methods: fundamentals and applications*. New York, NY: Wiley.

8. Zhang, L. L., & Zhao, X. S. (2009). Carbon-based materials as supercapacitor electrodes. *Chemical Society Reviews*, *38*(9), 2520-2531.

9. Zhong, C., Deng, Y., Hu, W., Qiao, J., Zhang, L., & Zhang, J. (2015). A review of electrolyte materials and compositions for electrochemical supercapacitors. *Chemical Society Reviews*, *44*(21), 7484-7539.

10. Gao, Q. (2013). *Optimizing carbon/carbon supercapacitors in aqueous and organic electrolytes* (Doctoral dissertation, Université d'Orléans).

11. Béguin, F., Presser, V., Balducci, A., & Frackowiak, E. (2014). Carbons and electrolytes for advanced supercapacitors. *Advanced Materials*, *26*(14), 2219-2251.

12. Abbas, Q., Pajak, D., Frąckowiak, E., & Béguin, F. (2014). Effect of binder on the performance of carbon/carbon symmetric capacitors in salt aqueous electrolyte. *Electrochimica Acta*, *140*, 132-138.

13. Sun, X., Zhang, X., Zhang, H., Huang, B., & Ma, Y. (2013). Application of a novel binder for activated carbon-based electrical double layer capacitors with nonaqueous electrolytes. *Journal of Solid State Electrochemistry*, *17*(7), 2035-2042.

14. Drobny, D. M., Tychyna, S. A., Maletin, Y. A., Stryzhakova, N. G., & Zelinskyi, S. A. (2013). Methods for manufacturing carbon electrodes for supercapacitors: Pros and Cons. In *Proceedings of the International Conference Nanomaterials: Applications and Properties* (No. 2, no. 4, pp. 04NEA17-04NEA17). Sumy State University Publishing.

15. Zhong, H., Sun, M., Li, Y., He, J., Yang, J., & Zhang, L. (2016). The polyacrylic latex: an efficient water-soluble binder for LiNi1/3Co1/3Mn1/3O2 cathode in li-ion batteries. *Journal of Solid State Electrochemistry*, *20*(1), 1-8.

16. Pan, J., Xu, G., Ding, B., Han, J., Dou, H., & Zhang, X. (2015). Enhanced electrochemical performance of sulfur cathodes with a water-soluble binder. *RSC Advances*, *5*(18), 13709-13714.

17. Simon, P., & Gogotsi, Y. (2008). Materials for electrochemical capacitors. *Nature Materials, 7*(11), 845-854.

18. Gu, W., & Yushin, G. (2014). Review of nanostructured carbon materials for electrochemical capacitor applications: advantages and limitations of activated carbon, carbide-derived carbon, zeolite-templated carbon, carbon aerogels, carbon nanotubes, onion-like carbon, and graphene. *Wiley Interdisciplinary Reviews: Energy and Environment*, *3*(5), 424-473.

19. Rodriguez-Reinoso, F., & Molina-Sabio, M. (1992). Activated carbons from lignocellulosic materials by chemical and/or physical activation: an overview. *Carbon*, *30*(7), 1111-1118.

20. Marsh, H., & Reinoso, F. R. (2006). *Activated carbon* (pp. 322-365). Elsevier.

21. Caturla, F., Molina-Sabio, M., & Rodriguez-Reinoso, F. (1991). Preparation of activated carbon by chemical activation with ZnCl2. *Carbon*, *29*(7), 999-1007.

22. Rufford, T. E., Hulicova-Jurcakova, D., Khosla, K., Zhu, Z., & Lu, G. Q. (2010). Microstructure and electrochemical double-layer capacitance of carbon electrodes prepared by zinc chloride activation of sugar cane bagasse. *Journal of Power Sources*, *195*(3), 912-918.

23. Ma, Y. (2017). Comparison of activated carbons prepared from wheat Straw via ZnCl2 and KOH Activation. *Waste and Biomass Valorization*, *8*(3), 549-559.

24. Ahmadpour, A., & Do, D. D. (1996). The preparation of active carbons from coal by chemical and physical activation. *Carbon*, *34*(4), 471-479.

25. Duman, G., Onal, Y., Okutucu, C., Onenc, S., & Yanik, J. (2009). Production of activated carbon from pine cone and evaluation of its physical, chemical, and adsorption properties. *Energy & Fuels*, *23*(4), 2197-2204.

26. Haykırı-Açma, H. (2003). Combustion characteristics of different biomass materials. *Energy Conversion and Management*, *44*(1), 155-162.

27. Özhan, A., Şahin, Ö., Küçük, M. M., & Saka, C. (2014). Preparation and characterization of activated carbon from pine cone by microwave-induced ZnCl2 activation and its effects on the adsorption of methylene blue. *Cellulose*, *21*(4), 2457-2467.

28. Karthikeyan, K., Amaresh, S., Lee, S. N., Sun, X., Aravindan, V., Lee, Y. G., & Lee, Y. S. (2014). Construction of high-energy-density supercapacitors from pine-cone-derived high-surface-area carbons. *ChemSusChem*, *7*(5), 1435-1442.

29. Rouquerol, J., Rouquerol, F., Llewellyn, P., Maurin, G., & Sing, K. S. (2013). *Adsorption by powders and porous solids: principles, methodology and applications* (pp. 52-90). London, UK: Academic Press.

30. Bansal, R. C., & Goyal, M. (2005). *Activated carbon adsorption* (pp. 67-141). Boca Raton, FL: CRC press.

31. Langmuir, I. (1918). The adsorption of gases on plane surfaces of glass, mica and platinum. *Journal of the American Chemical society*, *40*(9), 1361-1403.

32. Brunauer, S., Emmett, P. H., & Teller, E. (1938). Adsorption of gases in multimolecular layers. *Journal of the American Chemical Society*, *60*(2), 309-319.

33. Kaneko, K., Ishii, C., & Ruike, M. (1992). Origin of superhigh surface area and microcrystalline graphitic structures of activated carbons. *Carbon*, *30*(7), 1075-1088.

34. Centeno, T. A., & Stoeckli, F. (2010). The assessment of surface areas in porous carbons by two model-independent techniques, the DR equation and DFT. *Carbon*, *48*(9), 2478-2486.

35. Elmouwahidi, A., Bailón-García, E., Pérez-Cadenas, A. F., Maldonado-Hódar, F. J., & Carrasco-Marín, F. (2017). Activated carbons from KOH and H3PO4-activation of olive residues and its application as supercapacitor electrodes. *Electrochimica Acta*, *229*, 219-228.

36. Tuinstra, F., & Koenig, J. L. (1970). Raman spectrum of graphite. *The Journal of Chemical Physics*, *53*(3), 1126-1130.

37. Colthup, N. (2012). *Introduction to infrared and Raman spectroscopy* (pp. 1-68). New York, NY: Academic Press.

38. Shen, W., Li, Z., & Liu, Y. (2008). Surface chemical functional groups modification of porous carbon. *Recent Patents on Chemical Engineering*, *1*(1), 27-40.

39. Shi, H. (1996). Activated carbons and double layer capacitance. *Electrochimica Acta*, *41*(10), 1633-1639.

40. Barbieri, O., Hahn, M., Herzog, A., & Kötz, R. (2005). Capacitance limits of high surface area activated carbons for double layer capacitors. *Carbon*, *43*(6), 1303-1310.

41. Eliad, L., Salitra, G., Soffer, A., & Aurbach, D. (2001). Ion sieving effects in the electrical double layer of porous carbon electrodes: estimating effective ion size in electrolytic solutions. *The Journal of Physical Chemistry B*, *105*(29), 6880-6887.

42. Gamby, J., Taberna, P. L., Simon, P., Fauvarque, J. F., & Chesneau, M. (2001). Studies and characterisations of various activated carbons used for carbon/carbon supercapacitors. *Journal of Power Sources*, *101*(1), 109-116.

43. Chmiola, J., Yushin, G., Gogotsi, Y., Portet, C., Simon, P., & Taberna, P. L. (2006). Anomalous increase in carbon capacitance at pore sizes less than 1 nanometer. *Science*, *313*(5794), 1760-1763.

44. Largeot, C., Portet, C., Chmiola, J., Taberna, P. L., Gogotsi, Y., & Simon, P. (2008). Relation between the ion size and pore size for an electric double-layer capacitor. *Journal of the American Chemical Society*, *130*(9), 2730-2731.

45. Chmiola, J., Largeot, C., Taberna, P. L., Simon, P., & Gogotsi, Y. (2008). Desolvation of ions in subnanometer pores and its effect on capacitance and double-layer theory. *Angewandte Chemie*, *120*(18), 3440-3443.

46. Mysyk, R., Raymundo-Pinero, E., & Béguin, F. (2009). Saturation of subnanometer pores in an electric double-layer capacitor. *Electrochemistry Communications*, *11*(3), 554-556.

47. Mysyk, R., Raymundo-Piñero, E., Pernak, J., & Béguin, F. (2009). Confinement of symmetric tetraalkylammonium ions in nanoporous carbon electrodes of electric double-layer capacitors. *The Journal of Physical Chemistry C*, *113*(30), 13443-13449.

48. Ania, C. O., Pernak, J., Stefaniak, F., Raymundo-Piñero, E., & Béguin, F. (2009). Polarization-induced distortion of ions in the pores of carbon electrodes for electrochemical capacitors. *Carbon*, *47*(14), 3158-3166.

49. Abioye, A. M., & Ani, F. N. (2015). Recent development in the production of activated carbon electrodes from agricultural waste biomass for supercapacitors: a review. *Renewable and Sustainable Energy Reviews*, *52*, 1282-1293.

50. Subramanian, V., Luo, C., Stephan, A. M., Nahm, K. S., Thomas, S., & Wei, B. (2007). Supercapacitors from activated carbon derived from banana fibers. *The Journal of Physical Chemistry C*, *111*(20), 7527-7531.

51. Rufford, T. E., Hulicova-Jurcakova, D., Zhu, Z., & Lu, G. Q. (2008). Nanoporous carbon electrode from waste coffee beans for high performance supercapacitors. *Electrochemistry Communications*, *10*(10), 1594-1597.

52. Rufford, T. E., Hulicova-Jurcakova, D., Fiset, E., Zhu, Z., & Lu, G. Q. (2009). Double-layer capacitance of waste coffee ground activated carbons in an organic electrolyte. *Electrochemistry Communications*, *11*(5), 974-977.

53. Brunauer, S., Deming, L. S., Deming, W. E., & Teller, E. (1940). On a theory of the van der Waals adsorption of gases. *Journal of the American Chemical society*, *62*(7), 1723-1732.

54. Khalili, N. R., Campbell, M., Sandi, G., & Golaś, J. (2000). Production of micro-and mesoporous activated carbon from paper mill sludge: I. Effect of zinc chloride activation. *Carbon*, *38*(14), 1905-1915.

55. Liou, T. H. (2010). Development of mesoporous structure and high adsorption capacity of biomass-based activated carbon by phosphoric acid and zinc chloride activation. *Chemical Engineering Journal*, *158*(2), 129-142.

56. Lua, A. C., & Yang, T. (2005). Characteristics of activated carbon prepared from pistachio-nut shell by zinc chloride activation under nitrogen and vacuum conditions. *Journal of Colloid and Interface Science*, *290*(2), 505-513.

57. Shin, S., Jang, J., Yoon, S. H., & Mochida, I. (1997). A study on the effect of heat treatment on functional groups of pitch based activated carbon fiber using FTIR. *Carbon*, *35*(12), 1739-1743.

58. Figueiredo, J. L., Pereira, M. F. R., Freitas, M. M. A., & Orfao, J. J. M. (1999). Modification of the surface chemistry of activated carbons. *Carbon*, *37*(9), 1379-1389.

59. Dandekar, A., Baker, R. T. K., & Vannice, M. A. (1998). Characterization of activated carbon, graphitized carbon fibers and synthetic diamond powder using TPD and DRIFTS. *Carbon*, *36*(12), 1821-1831.

60. Seredych, M., Hulicova-Jurcakova, D., Lu, G. Q., & Bandosz, T. J. (2008). Surface functional groups of carbons and the effects of their chemical character, density and accessibility to ions on electrochemical performance. *Carbon*, *46*(11), 1475-1488.

61. Lazzarini, A., Piovano, A., Pellegrini, R., Leofanti, G., Agostini, G., Rudić, S. (2016). A comprehensive approach to investigate the structural and surface properties of activated carbons and related Pd-based catalysts. *Catalysis Science & Technology*, *6*(13), 4910-4922.

62. Ferrari, A. C., & Robertson, J. (2000). Interpretation of Raman spectra of disordered and amorphous carbon. *Physical Review B*, *61*(20), 14095.

63. Dillon, R. O., Woollam, J. A., & Katkanant, V. (1984). Use of Raman scattering to investigate disorder and crystallite formation in as-deposited and annealed carbon films. *Physical Review B*, *29*(6), 3482.

64. Fung, A. W. P., Rao, A. M., Kuriyama, K., Dresselhaus, M. S., Dresselhaus, G., Endo, M., & Shindo, N. (1993). Raman scattering and electrical conductivity in highly disordered activated carbon fibers. *Journal of Materials Research*, *8*(3), 489-500.

65. Mrozowski, S. (1971). Electronic properties and band model of carbons. *Carbon*, *9*(2), 97-109.

66. Pandolfo, A. G., & Hollenkamp, A. F. (2006). Carbon properties and their role in supercapacitors. *Journal of Power Sources*, *157*(1), 11-27.

67. Zhao, J., Dai, Y., Xu, J., Chen, S., & Xie, J. (2008). Synthesis and electrochemical characterization of mesoporous carbons prepared by chemical activation. *Journal of the Electrochemical Society*, *155*(7), A475-A480.

68. Stoller, M. D., & Ruoff, R. S. (2010). Best practice methods for determining an electrode material's performance for ultracapacitors. *Energy & Environmental Science*, *3*(9), 1294-1301.